RESEARCH PAPER

Acta Neurobiol Exp 2020, 80: 225–244
DOI: 10.21307/ane-2020-021

RhoA/Rock2/Limk1/cofilin1 pathway is involved in attenuation of neuronal dendritic spine loss by paeonol in the frontal cortex of *D*-galactose and aluminum-induced Alzheimer's disease-like rat model

Fei Han[1], Hui Xu[1,2], Jun-Xian Shen[1], Chuan Pan[1], Zong-Hao Yu[1], Jing-Jing Chen[1], Xiu-Ling Zhu[1,3], Ya-Fei Cai[1] and Ya-Ping Lu[1]*

[1] College of Life Science, Anhui Normal University, Wuhu, China, [2] Anhui College of Traditional Chinese Medicine, Wuhu, China, [3] Department of Anatomy, Wannan Medical College, Wuhu, China,

** Email: yapinglu@ahnu.edu.cn*

Alzheimer's disease (AD) has become the most prevalent neurodegenerative disorder. Given the pathogenesis of AD is unclear, there is currently no drug approved to halt or delay the progression of AD. Therefore, it is pressing to explore new targets and drugs for AD. In China, polyphenolic Chinese herbal medicine has been used for thousands of years in clinical application, and no toxic effects have been reported. In the present study, using *D*-galactose and aluminum-induced rat model, the effects of paeonol on AD were validated *via* the Morris water maze test, open field test, and elevated plus maze test. Neuronal morphology in frontal cortex was assessed using ImageJ's Sholl plugin and RESCONSTRUCT software. RhoA/Rock2/Limk1/cofilin1 signaling pathway-related molecules were determined by Western blotting. Cofilin1 and p-cofilin1 were analyzed by immunofluorescence. Results showed that pre-treatment with paeonol attenuated *D*-galactose and aluminum-induced behavioral dysfunction and AD-like pathological alterations in the frontal cortex. Accompanied by these changes were the alterations in the dendrite and dendritic spine densities, especially the mushroom-type and filopodia-type spines in the apical dendrites, as well as actin filaments. In addition, the activity and intracellular distribution of cofilin1 and the molecules RhoA/Rock2/Limk1 that regulate the signaling pathway for cofilin1 phosphorylation have also changed. Our data suggests that paeonol may be through reducing Aβ levels to alleviate the loss of fibrillar actin and dendrites and dendritic spines *via* the Rho/Rock2/Limk1/cofilin1 signaling pathway in the frontal cortex, and ultimately improving AD-like behavior.

Key words: Alzheimer's disease, frontal cortex, dendritic spine, cofilin1, RhoA, Rock2, Limk1

INTRODUCTION

Dementia is one of the major causes of disability and dependency among older people worldwide. Every year, there are nearly 10 million new cases (WHO, 2019). Alzheimer disease (AD) is the most common form of dementia and may account for 60–70% of cases (Tang et al., 2016). The early clinical symptoms of the disease are mainly cognitive impairment such as memory and visuo-spatial skills, and then gradually worsen, accompanied by emotional behavioral reactions such as depression, anxiety, and decreased activity (Lyketsos et al., 2011; Ameen-Ali et al., 2017; Götz et al., 2018).

The typical histopathological hallmarks of AD are the aggregation of amyloid-beta in extracellular senile plaques, accumulation of tau in intracellular neurofibrillary tangles, and neuron loss, in the brain especially in hippocampus and frontal cortex (Hyman et al., 2012; Grontvedt et al., 2018; Alzheimer's Association, 2019). However, the etiology and pathogenesis of AD are un-

Received 2 December 2019, accepted 19 April 2020

clear. A number of studies have revealed that AD undergoes a progressive lesion process and is thought to begin 20 years or more before symptoms arise, with small changes in the brain (Jack et al., 2009; Heiko et al., 2011; Bateman et al., 2012; Reiman et al., 2012; Villemagne et al., 2013; Gordon et al., 2018). Only the brain synapses and neurons involved in thinking, learning, and memory (cognitive function) have been damaged or destroyed, and AD shows symptoms (Alzheimer's Association, 2019). Clinical histopathological studies have demonstrated that in layer II and III pyramidal neuron dendrites, spine density is similar among controls and CAD cases (cognitively normal individuals with high AD pathology) but is reduced significantly in AD dementia cases, suggesting a close relationship between symptoms and spines, the postsynaptic component (Boros et al., 2017). Accordingly, it is proposed that pathology characterized by Aβ and hyperphosphorylated-tau occurs in early AD, but does not cause significant damage and loss of synapses and neurons, and therefore does not exhibit AD symptoms; but over time, Aβ synergizes with hyperphosphorylated-tau, causing significant dendrite and synaptic loss, which in turn shows symptoms of AD (Ittner and Ittner, 2018; Alzheimer's Association, 2019) .

Given the pathogenesis of AD remains to be illustrated, there is currently no drug approved to halt or delay the progression of AD (Anderson et al., 2017). With the failure of phase 3 clinical trials for the treatment of AD drugs in recent years, including the β secretase inhibitor verubecestat (Egan et al., 2018) and the anti-Aβ drugs semagacestat (Doody et al., 2013), bapineuzumab (Vandenberghe et al., 2016) and solanezumab (Neurology, 2017), it is even more important to explore new targets and drugs.

In China, polyphenolic Chinese herbal medicine has been used for thousands of years in clinical application, and no toxic effects have been reported (Zhang et al., 2019). Polyphenols are usually easily absorbed by the gastrointestinal tract and quickly cross the blood-brain barrier (Lin, 2011). Paeonol (Pae, 20-hydroxy-40--methoxyacetophenone), a simple phenolic compound, is the main active component extracted from Moutan cortex and *Cynanchum paniculatum.* A lines of studies have shown that paeonol has various biological and pharmacological activities including anti-inflammation (Tz-Chong et al., 2003; Ishiguro et al., 2006), antioxidation (Liu et al., 2017), anti-neurotoxicity (Liu et al., 2018), anti-tumor effects (Hagen et al., 2003; Kubes and Mehal, 2012), and anti-anxiety (Ishiguro et al., 2006), as well as anti-diabetic effects (Lau et al., 2007), anti-hyperglycemic effects (Juan et al., 2010) and protection of rat heart (Ma et al., 2016).

The latest researches reveal that paeonol can inhibit oxidized low-density lipoprotein-induced vascular endothelial cells autophagy by upregulating the expression of miRNA-30a (Li et al., 2018a), ameliorate diabetic renal fibrosis through promoting the activation of the Nrf2-ARE pathway *via* up-regulating sirt1 (Zhang et al., 2018), attenuate the inflammatory responses of endothelial cells *via* stimulating monocytes-derived exosomal microRNA-22 (Liu et al., 2018), and ameliorate glucose and lipid metabolism in experimental diabetes by activating Akt (Xu et al., 2019). In addition, paeonol has an anti-atherosclerotic effect against vascular smooth muscle cell proliferation by up-regulation of autophagy *via* the AMPK-mTOR signaling pathway (Wu et al., 2017), prevents bleomycin-induced pulmonary inflammation and fibrosis in mice through the inhibition of the MAPKs/Smad3 signaling (Liu et al., 2017), and alleviate nerve damage caused by intracerebral hemorrhage by activating the PI3K/AKT pathway (Li et al., 2018b). Our previous study shows that paeonol can attenuate D-galactose and aluminum-induced dendritic damage in the hippocampus (Han et al., 2017). In this study, we found involvement of Rho/Rock2/Limk1/cofilin1 pathway in paeonol's attenuation of neuronal dendritic loss in the frontal cortex of *D*-galactose and aluminum-induced rat model of Alzheimer's disease.

METHODS

Reagents and Drugs

The chemical structure of paeonolsilate sodium ($C_9H_9NaO_6S$, a derivative of paeonol) was shown in Fig. 1. Paeonolsilatie sodium injection (0.1g/2 ml), which has the same pharmacological effects as paeonol and has been approved by the Chinese FDA for clinical use in the treatment of muscle pain, arthralgia, rheumatism, neuralgia and abdominal pain (No.H20064790, http://app1.sfda.gov.cn/datasearchcnda/face3/dir.html), was purchased from Jinling Pharmaceutical Company (Nanjing, China). *D*-galactose (*D*-gal) was purchased from

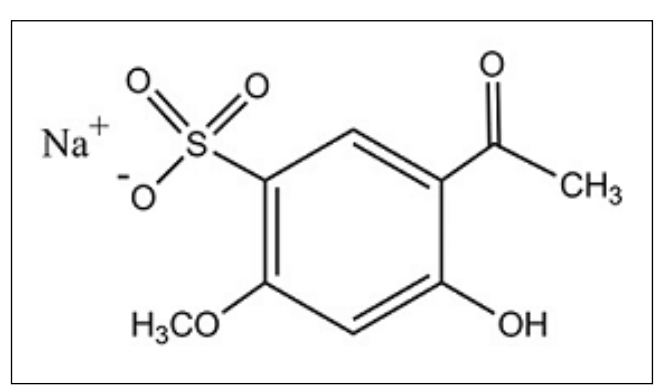

Fig. 1. The structural formula of paeonolsilate sodium.

Sangon Biotech (Shanghai, China). Aluminum ($AlCl_3$) was purchased from Guangzhou Chemical Reagent Factory (Guangzhou, China). Phospho-Tau (Ser202) and $A\beta_{1-42}$ antibodies (used to recognize the Aβ fibrils) were purchased from Bioss Biological Technology Co., Ltd (Beijing, China). RHOA antibody was purchased from Sangon Biological Technology Co., Ltd (Shanghai, China). LIMK1, ROCK2 and PI3K antibodies was purchased from Boster Biological Technology Co., Ltd (Wuhan, China). A11 antibody (used to recognize the Aβ oligomers, SAB5200113) was purchased from Sigma-Aldrich (St. Louis, USA). Cofilin1, SSH1 antibodies and DAPI were purchased from Santa Cruz Biotechnology. Other chemicals were purchased from Sigma.

Animals and Treatments

Adult male Sprague-Dawley (SD) rats (180–200 g) were obtained from the Shandong Experimental Animal Center (license number, SCXK20140007; Jinan, China) and housed at 20 ± 2°C, with a light cycle between 08:00 and 20:00 h. Food and water were provided *ad libitum*. Animals were treated according to the Guidelines of the Regulations of Experimental Animal Administration issued by the State Committee of Science and Technology of the People's Republic of China on November 14, 1988. All animal experiments were conducted with the approval of the Animal Use and Care Committee of Anhui Normal University (2015002).

$AlCl_3$ and *D*-gal co-induced animal models may be used to characterize AD-like behavioral and pathological features, as well as pathologic processes without the genetic background of gene mutations and have thus been widely used in AD-related studies (Sun et al., 2009; Lu et al., 2017; Wei et al., 2017; Xiao et al., 2017; Chiroma et al., 2019). In this study, D-gal was dissolved in physiologic saline (0.9%) and injected (100 mg/kg/day, once per day, s.c.). $AlCl_3$ was dissolved in double-distilled water and administered (40 mg/kg/day, once per day, i.g.). Model induction lasted for 42 days.

Following a one-week adaptation period, thirty male rats were randomly divided into 3 groups of 10 rats each: the control group (CON), *D*-gal + $AlCl_3$ group (DGA group treated with *D*-gal + $AlCl_3$ for 42 days), Paeononlsilatie sodium treatment group (PEA group treated with 50 mg/kg, i.p., 1 h before *D*-gal + $AlCl_3$ for 42 days). The control treatments were volume-matched vehicle.

Behavioral tests

Rats were brought to the testing room 30 min before the start of each behavioral test and remained in the same room through the test. All behavioral tests were performed during the light cycle under lighting condition in 70 lx by experimenters blind to treatment information.

Open field test (OFT)

The OFT is a well-established paradigm to examine fear in rodents (Walsh and Cummins, 1976). The test apparatus was made of opaque materials into lidless boxes with length, width and height of 80 cm × 80 cm × 40 cm respectively. The bottom was divided into 25 quadrates of 16 cm × 16 cm by a white line. First, the rats were placed in the laboratory 30 min prior to testing to adapt to the environment. And then, each rat was placed in the center area, which was defined as 9 squares in the center, and the behaviors were recorded for 5 min in a quiet environment. The number of squares crossed, number of clean movements, and number of rears were recorded. The observers were blind to the rats of the different treatment groups. The device was cleaned with 70% ethanol thoroughly after each trial.

Elevated plus maze test (EPMT)

The EPMT was commonly used to assess anxiety behaviors (Pellow et al., 1985). The high cross apparatus consisted of four black arms (50 cm × 10 cm) and a central square platform (10 cm × 10 cm). Two of the arms were closed arms with walls (40 cm height), called the closed arms. And the other two arms were open without walls, called the open arms. The maze was elevated 50 cm from the floor. There was a camera right above it. The animals were placed individually at the center of the maze, facing one of the open arms, and their activities were recorded for 5 min. When a rat placed its four paws into an arm, it was counted as entry in the arm. Recordings were made of the time spent in the open arms, the time spent in the closed arms, and the number of head dipping. The maze was cleaned with 70% ethanol thoroughly after each trial. The experimenters who recorded the data were unaware of the grouping.

Morris water maze test (MWMT)

The MWMT, which was usually used to assess spatial learning and memory capability, was carried out according to methods described previously (Morris, 1984; Vorhees and Williams, 2006). The pool (1.5 m in diameter, 50 cm in height) was filled with water to a depth of 30 cm. A circular escape platform (15 cm in diameter) was submerged 2 cm below the water surface. The

water was clouded with black food coloring to prevent the visual image of the submerged platform. Rats were trained to find a hidden platform in a water maze for five consecutive days. For each trial, the rat was placed facing the wall at one of four designated start points. Each rat was allowed to find the platform for 60 s and remained on the platform for 20 s. If he could not reach the platform within 60 s, he was guided gently to the platform and escape latency (time taken to find the platform) was recorded as 60 s. The rat stayed on the platform for 20 s. The average escape latencies of the four trials per day were used for statistical analysis. A longer time spent in finding the platform was used to assess the extent of learning impairment.

A probe trial without the platform was performed twenty-four hours after the final acquisition trial. During probe trials, the animals were allowed to swim for 60 s within the pool while their time spent in the target quadrant was recorded. The longer a rat stayed in the target quadrant, the better it scored for spatial memory.

The swimming behaviors of each rat were monitored *via* a television camera mounted overhead. The time was manually recorded with a stopwatch by two observers. Modeling, treatment and behavioral test schedule were shown in Fig. 2.

Tissue preparation

Twenty-four hours after the behavioral tests, the rats were deeply anesthetized with 1% carbrital and perfused (*via* a transcardial approach) with 0.9% saline. And then, rats were treated according to the requirements of different experimental methods. Six rats of each group were euthanasia *via* decapitation and the half frontal cortex tissue of which was stored in Golgi-cox solution, while the other half of which was stored in a -80°C refrigerator for further Western blot analysis. Four rats in each group, perfused with 4% paraformaldehyde and euthanasia, followed by the frontal cortex tissues being collected and embedded in paraffin wax. The paraffin-embedded tissues were cut with a Leica microtome (RM2235) into serial coronal sections (6 μm).

Golgi-Cox staining

The Golgi–Cox staining was mainly based on our previous papers (Han et al., 2017; Zhu et al., 2018). Briefly, frontal cortex tissues were stored in Golgi-Cox solution in the dark at 37°C for 48 h and subsequently sectioned (200 μm thick coronal sections) using a vibratome (NVSL/NVSLM1). The sections were then immersed in alcohol (50%) for 5 min, ammonium hydroxide for 5±10 min, and 5% sodium thiosulfate in the dark for 10 min and serially dehydrated in solute alcohol, including 70%, 80%, and 95% alcohol (7 min × 2 for each) and 99% 1-butanol for 7 min; the samples were subsequently cleaned in xylene for 5 min and medium mounted with coverslips using Rhamsan gum.

Immunohistochemistry

Coronal sections (6 μm) of the brain samples were rinsed with PBS over 5 min and subsequently blocked

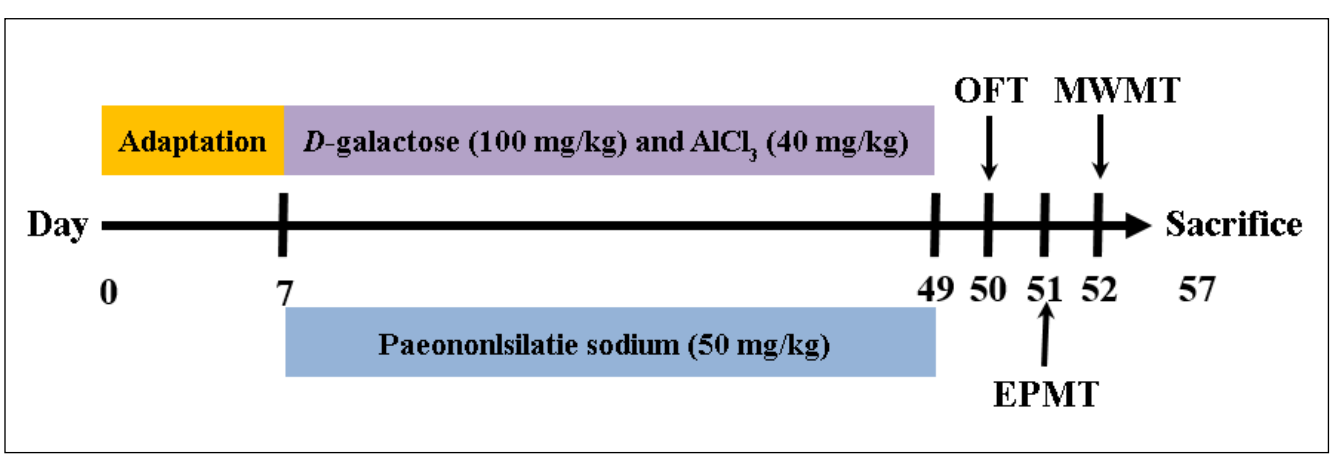

Fig. 2. Schematic diagram of the timeline for establishing an AD model, treatment and behavioral test. The upper yellow rectangular box indicated adaptation treatment from day 0 to day 7. The upper purple rectangular box or down blue rectangular box indicated the treatment with *D*-gal and $AlCl_3$ or Paeononlsilatie sodium from day 8 to day 49, respectively. Paeononlsilatie sodium was given 1 h before *D*-gal and $AlCl_3$ treatment. The downward or upward arrows indicated the rats performed for the behavioral test. OFT, open field test; EPMT, elevated plus maze test; MWMT, Morris water maze test. The rats were sacrificed on day 57.

for 30 min at room temperature in PBS-Triton (0.1 M PBS and 0.3% Triton X 100). After blocking, samples were subsequently treated twice (2 × 10 min) by microwaves (700 W) in 0.05 M citrate buffered saline (pH 6.0). After being washed in PBS, the samples were blocked with normal bovine serum in PBS for 1 h at 37°C, followed by incubation with primary antibodies (rabbit $A\beta_{1-42}$ pA (1:200), rabbit phospho-tau (p-tau) pA (1:200) or mouse cofilin1 mA (1:200) overnight at 4°C. Single labeling with DAB ($A\beta_{1-42}$ and p-tau immunoreactivity): after being washed, the sections were incubated with the secondary antibody goat anti-rabbit (Boster Biotech, Wuhan, China) for 1 h at 37°C. Double labeling with fluorescein labeling methods previously described by our group (Ya-Ping et al., 2003). Sections were then washed over 5 min two times with PBS and incubated with the secondary antibody biotinylated horse anti-mouse IgG diluted in PBS (1:200) that contained 5% normal horse serum for 1 h at 37°C, which was performed as previously described (Hu et al., 2003; Han et al., 2017). Then these sections were incubated with Cy™3-labeled streptavidin (Kirkegaard and Perry Laboratories) diluted in PBS for 30 min at room temperature, followed by incubation with 0.05 M glycine-HCl buffer saline (pH 2.2) for 2 h at room temperature to quench additional antibodies; the samples were subsequently incubated with second primary antibodies against rabbit p-cofilin1 pA (1:200) for 24 h at 4°C and incubated with the fluorescein isothiocyanate (FITC)-conjugated goat anti-rabbit IgG (Vector Laboratories, Burlingame, CA) for 1 h, diluted in PBS (1:100). Then sections incubation with DAPI for 10 min. Finally, the sections were cover slipped with glycerin. Control samples were simultaneously performed following the same procedures as the test samples with the exception that the primary antibodies were omitted.

Images were obtained with an Olympus FV1000 laser scanning confocal microscope. FV10-ASW 4.2 Viewer software was used for image format conversion. To assess the distribution of cofilin1 in neurons, plots of florescence intensity *versus* distance were generated using the RGB profile plot function (intensity line profile for red channel) of ImageJ 1.49 s (NIH).

Western blotting

Briefly, 10% (w/v) tissue homogenates were centrifuged at 12,000×g for 30 min at 4°C, and the supernatants were transferred to clean tubes and stored. Protein concentration was determined using the bicinchoninic acid assay. The proteins (40 μg of total protein) were electrophoresed on various concentrations of Tris-tricine polyacrylamide gels (under non reducing conditions) and transferred onto PVDF membranes. The blots were blocked with 5% nonfat dry milk in Tris-buffered saline Tween 20 (TBS-T) for 2 h at room temperature. Then, membranes were incubated with antibodies (Table I) were diluted in 0.1% BSA/TBS-T, covered with plastic wrap and incubated for 12 h at 4°C. Bound antibodies were visualized with horseradish peroxidase-conjugated secondary antibodies and the ECL detection system (BEYOTIME Biological Technology Co., Ltd, China). Densitometric analysis of antibody specific bands was performed with NIH ImageJ version 1.34 software.

Image analysis

Image analysis and quantification of the histological sections were performed by one author who was not aware of the experimental information. Images were captured under Laser scanning confocal microscope (OLYMPUS FV1000) and analyzed using image analysis software (ImageJ). In serial sections between bregma +2.22 mm and +1.98 mm, one section was selected at intervals of every sixth section. In frontal cortex, three fields of view (×60 objective) were randomly selected for accounting the number of p-tau immnopositive cells and the percentage of the field of view covered by $A\beta_{1-42}$. In frontal cortex layer III, three fields of view (×60 objective) each region (in the basal dendritic region and the apical dendritic region of pyramidal cells) were randomly selected for the further statistics in the percentage of the field of view covered by fibrillary actin as described previously (Han et al., 2017).

Table I. Antibodies and dilution ratio.

Antibody	Dilution ratio
p-cofilin1 (Ser3)	1:1000
Cofilin1	1:500
SSH1	1:400
RHOA	1:500
LIMK1	1:300
ROCK2	1:250
PI3K	1:300
GAPDH	1:400
HRP-conjugated Goat Anti-Rabbit IgG	1:5000
HRP-conjugated Goat Anti Mouse IgG	1:4000
H&L conjugated Goat Anti-Rabbit IgG	1:1000

Quantification of Dendrites and Dendritic Spines

Measurements of the dendritic branch and length were based primarily on previous literature (Mavroudis et al., 2011; Lazcano et al., 2014). Briefly, the regions tested were determined at a low magnification according to the description by Paxinos and Watson (2006), and more than 5 neurons in the frontal cortex layer III per mouse were selected to acquire their photographs, which were used for quantificational analysis. The criteria used to select neurons for quantitative analysis have been previously described (Flores et al., 2005; Bringas et al., 2013; Lazcano et al., 2014). Each selected neuron was analyzed using ImageJ software. Neuronal branches were traced by the NeuronJ plug-in to count their total dendritic length, and dendritic intersections that cross the concentric circles were counted using the Sholl analysis plug-in protocol (Kolb et al., 1998; Flores et al., 2005; Martinez-Tellez et al., 2009).

The analysis of the density and classification of dendritic spines were mainly based on the methods described in the previous literatures (Sebastian et al., 2013; Foster et al., 2018). Concisely, three independent coronal sections at the same level of bregma's parameter per mouse were used for analysis. At the apical dendrites (>50 μm from the center of the neuronal body) and basal dendrites in frontal cortex layer III, secondary or tertiary dendritic segments of pyramidal neurons were selected for analysis. The number of neurons used for analysis in each section is not less than 10, and the total length of the dendritic segments is greater than 300 μm. Z-stacks of dendrites (up to 80 μm total on Z-axis; optical section thickness=0.5 mm, i.e., 160 images per stack) were obtained at 60 × 6 magnification on an OLYMPUS FV1000. RECONSTRUCT software was used to analyze the density and type of spines. Based on our previous literature (Han et al., 2017; Zhu et al., 2018), the analysis was divided into three steps: step 1, series import and calibration; step 2, dendritic segment identification and measurement; and step 3, spine measurement and classification. According to the literature (Risher et al., 2014), the dendritic spines were classified into three types based on the parameters as shown in Table II.

Table II. Classification of spine morphology using RECONSTRUCT software.

Type	Parameters
Mushroom spines	Mean_Width (head) > 0.6 μm
Stubby spines	Length : Width Ratio < 1 Length < 1 μm
Filopodia spines	Length > 0.6 μm

Statistical Analyses

In this study, one-way ANOVA followed by *post hoc* least-significant difference (LSD) was used for comparisons of more than three groups, and a two-tailed t test was used for comparisons between two groups. The data of the spatial navigation tasks and the Sholl analysis were analyzed by a repeated ANOVA followed by *post hoc* Bonferroni's multiple comparisons. All data was analyzed with SPSS v22.0 software (IBM, New York, NY, USA) and expressed as the mean ± standard error of the mean (SEM). $P<0.05$ was considered to be statistically significant.

RESULTS

Paeonol attenuated D-galactose and aluminum-induced Alzheimer's disease-like behavioral damage

In this study, the Morris water maze test (MWMT), open field test (OPT), and elevated plus maze test (EPMT) were used to evaluate the effects of paeonol on the learning and memory, locomotor activity, and anxiety emotion of rats, respectively. In the statistics of behavior data, animals whose behavior parameters were recorded incorrectly or whose video records were incomplete were excluded from the statistics. One-way ANOVA showed that paeonol significantly relieved *D*-galactose and aluminum-induced reduction in the number of squares crossed ($F_{2,25}=25.012$, $P<0.001$; *post hoc* comparisons: DGA *vs.* CON, $P<0.001$; PAE *vs.* DGA, $P<0.05$) (Fig. 3A) and the number of rearing movements ($F_{2,24}=32.627$, $P<0.001$; *post hoc* comparisons: DGA *vs.* CON, $P<0.001$; PAE *vs.* DGA, $P<0.001$) (Fig. 3B) in OPT, as well as reduction in the time spent open arms ($F_{2,24}=39.741$, $P<0.001$; *post hoc* comparisons: DGA *vs.* CON, $P<0.001$; PAE *vs.* DGA, $P<0.001$) (Fig. 3C) and increase in the time spent in closed arms ($F_{2,24}=39.741$, $P<0.001$; *post hoc* comparisons: DGA versus CON, $P<0.001$; PAE *vs.* DGA, $P<0.001$) (Fig. 3D) in EPMT.

In MWMT, Pillai's trace of the repeated ANOVA showed that there was no significant difference between day and group ($F_{2,26}=2.149$, $P>0.05$). Tests of between-subjects effects displayed a significant difference between groups in the escape latency ($F_{2,24}=6.120$, $P<0.01$). One-way ANOVA revealed differences between groups found on the day 4 ($F_{2,24}=7.563$, $P<0.01$) and 5 ($F_{2,24}=13.562$, $P<0.001$). Pairwise comparisons demonstrated that paeonol decreased *D*-galactose and aluminum-induced increase in the escape latency on the fourth day (DGA *vs.* CON, $P<0.001$; PAE *vs.* DGA, $P<0.01$) (Fig. 3E). The probe trial performances were assessed by removing the platform 24 h after the acquisition trials. The time spent in the region of target quadrant

around the platform showed a significant difference between the groups ($F_{2,24}$=9.848, P<0.01). *Post hoc* comparisons indicated that *D*-galactose and aluminum induced a marked reduction in the time spent in the area around the platform (P<0.001), which can be attenuated by treatment with paeonol (P<0.01) (Fig. 3F).

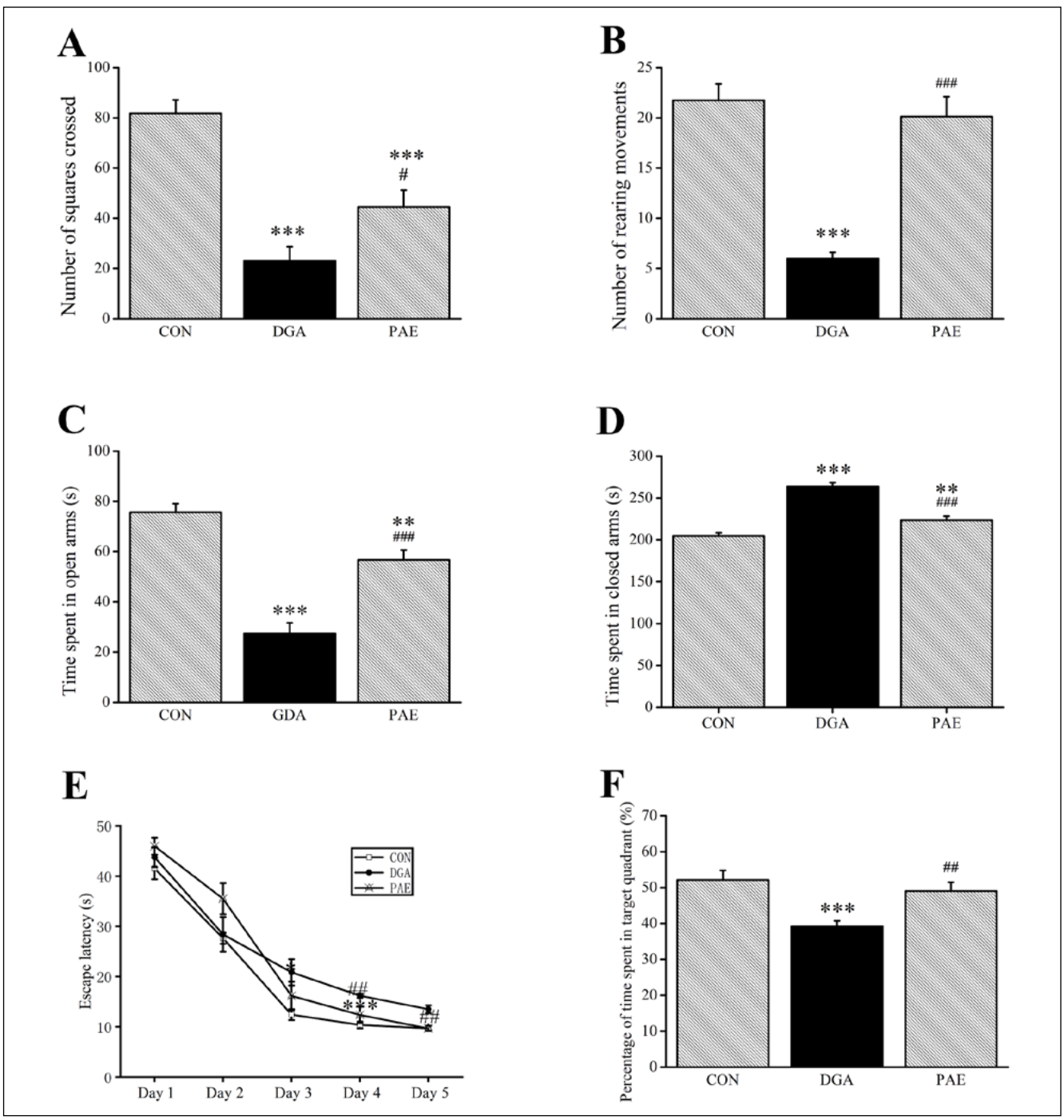

Fig. 3. Effects of paeonol on the behavioral performances in OFT (A, B), EPMT (C, D) and MWMT (E, F). Paeonol treatment (50 mg/kg, i.p.) attenuated the *D*-gal and AlCl3-induced decrease in the number of squares crossed (A) and the number of rearing movements (B) in the OFT. In the EPMT, *D*-gal and $AlCl_3$ induced a decrease in the time spent in open arms (C) and an increase in the time spent in closed arms (D), these of which were significantly improved by paeonol treatment. (E) The average escape latencies of four acquisition trials per day in DGA rats from days 4 to 5 were significantly more than those in CON rats. Paeonol pretreatment produced significant protective effects, particularly at days 4~5. (F) Probe trials 24 h after acquisition trials indicated that animals treated with paeonol spent more time in the target quadrant than animals in DGA. Data expressed as the means ± SEM (n=8-10). **P<0.01, ***P<0.001 *versus* CON; $^{\#}P$<0.05, $^{\#\#}P$<0.01, $^{\#\#\#}P$<0.001 *versus* DGA.

Paeonol decreased D-galactose and aluminum-induced increase of oligomeric Aβ and hyperphosphorylated-tau in the frontal cortex

Immunohistochemical examination showed that paeonol significantly attenuated *D*-galactose and aluminum-induced increase of oligomeric Aβ (Fig. 4A a, b, c) and hyperphosphorylated-tau (Fig. 4B a, b, c) in the frontal cortex. Two-tailed *t* test indicated that the percentage of Aβ immunopositive area in the visual field area (P<0.001) (Fig. 4A d) and the hyperphosphorylated-tau immunopositive cell number per visual field area (P<0.001) (Fig. 4B d) in PAE were markedly lower than that in the DGA.

Western blotting revealed that *D*-galactose and aluminum caused a noteworthy increase in oligomeric Aβ levels, which were downregulated by treatment with paeonol (Fig. 4C). Numerous studies have demonstrated that some types of Aβ oligomers have strong neurotoxicity, such as ~32 KD Aβ oligomers (Fernando et al., 2010;

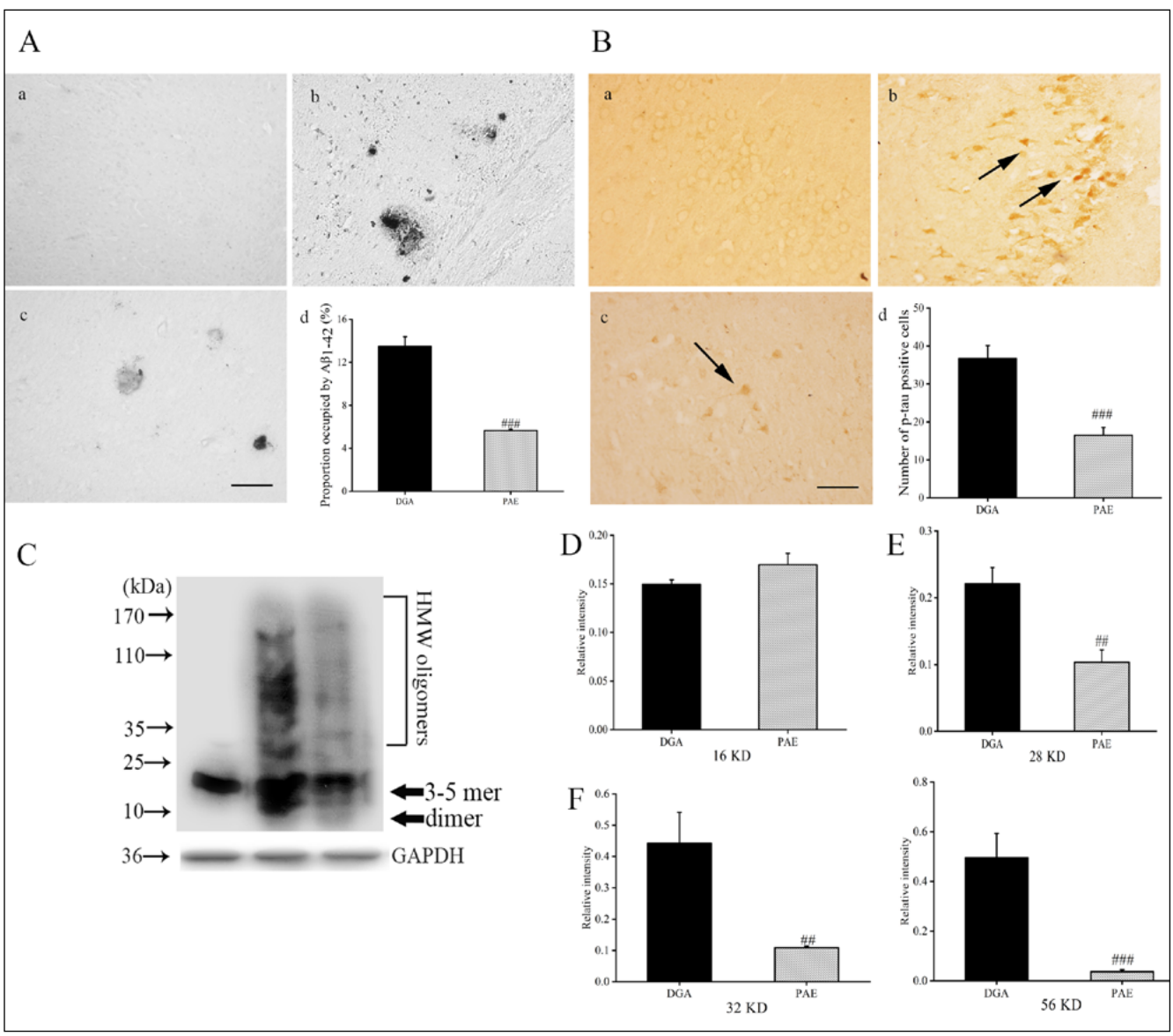

Fig. 4. Effects of Paeonol on *D*-gal and AlCl3-induced Aβ and tau burdens in the frontal cortex. (A) Grayscale microscope pictures in immunohistochemical staining with Aβ1-42 antibody in the frontal cortex in CON (a), DGA (b), and PAE (c); administration of paeonol (50 mg/kg, i.p.) for 6 weeks significantly reduced the percentage area of Aβ1-42-positive deposits (d). (B) Phospho-tau immunohistochmical staining (p-Ser 202) in the frontal cortex in CON (a), DGA (b), PAE (c), and their statistical analysis in the number of p-tau positive cells (d). (C) Western blot bands with A11 antibody identifying different molecular weights of Aβ oligomers in the frontal cortex in CON (left column), DGA (middle left column), PAE (middle right column). Paeonol did not affect the expression of 16 KD Aβ oligomers (D); however, it decreased the expression of 28 KD (E), 32 KD (F), and 56 KD Aβ oligomers (G). Data expressed as the means ± SEM (n=4~5). $^{\#\#}P$<0.01, $^{\#\#\#}P$<0.001 *versus* DGA. Scales: 50 μm in A (c) and B (c).

Yang et al., 2011; Washington et al., 2014), especially ~56 KD Aβ oligomers (Lesne et al., 2013). Therefore, we examined the effects of paeonol on the expression levels of 16 KD, 28 KD, 32 KD, and 56 KD. Two-tailed *t* test showed that paeonol treatment remarkably reduced Aβ oligomer levels in 28 KD (P<0.01), 32 KD (P<0.01), and 56 KD (P<0.001), but not in 16 KD (P>0.05).

Paeonol relieved D-galactose and aluminum-induced dendrite and dendritic spine loss in the frontal cortex

Excitatory synapses occur on dendritic protrusions called dendritic spines, and synapse activity is inseparably linked to spine density and morphology (Yasun-

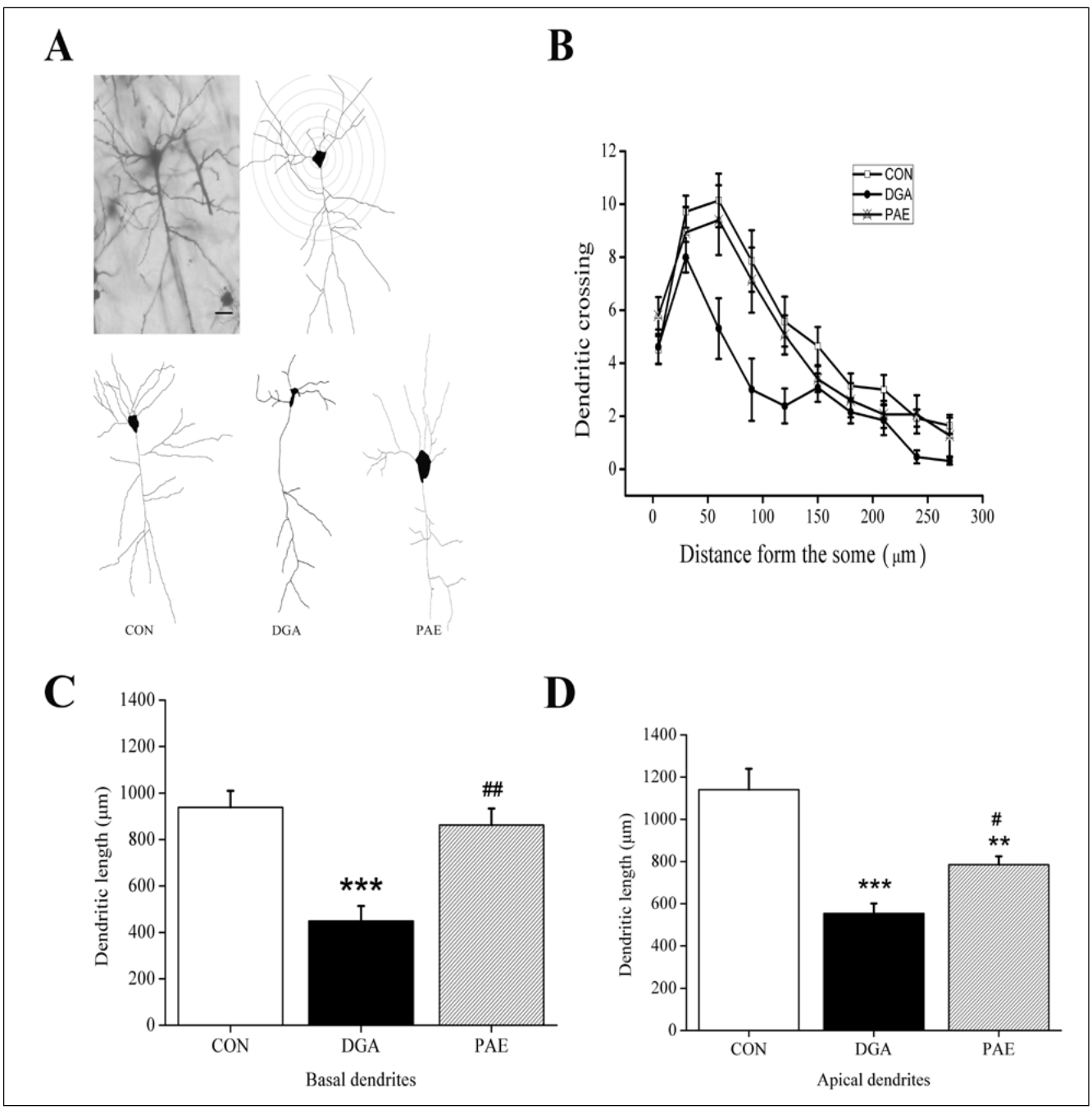

Fig. 5. Effects of Paeonol on the dendritic length and branches in frontal cortex. (A) Frontal cortex pyramidal neurons and their traces drawn by ImageJ software. Paeonol treatment (50 mg/kg, i.p.) for 6 weeks significantly increased the number of dendriticbranches (B), extended the length of basal dendrites (C), and increased the length of apical dendrites (D). Data expressed as the means ± SEM (n=5). **P*<0.05, ***P*<0.01, ****P*<0.001 *versus* CON; #*P*<0.05, ##*P*<0.01 *versus* DGA.

ori and Majewska, 2005). Dendritic spine and neuronal synapse loss correlate more strongly with cognitive impairment than classical pathologic markers of AD (Dekosky and Scheff, 1990; Terry et al., 2010). So, in this study, we evaluated the effects of paeonol on the dendrite and dendritic spine loss induced by *D*-galactose and aluminum in the frontal cortex.

As shown in Fig. 5A, the dendrites were traced for counting their length by the NeuronJ plug-in, and the dendritic intersections that cross the concentric circles were counted for the dendritic branches by the Sholl analysis plug-in protocol. One-way ANOVA indicated that significant differences of dendritic length between groups were found in the basal dendrites ($F_{2,14}$=19.085, P<0.001) and apical dendrites ($F_{2,14}$=15.781, P<0.001). *Post hoc* comparisons showed that there were remarkable differences between CON and DGA (P<0.001) and between DGA and PAE (P<0.01) in the basal dendrites (Fig. 5C), as well as between CON and DGA (P<0.001) and between DGA and PAE (P<0.01) in the apical dendrites (Fig. 5D). A repeated ANOVA revealed that the total dendritic intersections between groups existed dramatically different ($F_{2,14}$=9.714, P<0.001; *post hoc* comparisons: CON *vs.* DGA, P<0.001; PAE *vs.* CON, P<0.05; PAE *vs.* DGA, P<0.05). Segmentation statistics showed that the significant differences between the groups were found at some segments, especially at segment 3 ($F_{2,14}$=4.702, P<0.05; *post hoc* comparisons: CON *vs.* DGA, P<0.01; PAE *vs.* DGA, P<0.05), 4 ($F_{2,14}$=4.608, P<0.05; *post hoc* comparisons: CON *vs.* DGA, P<0.01; PAE *vs.* DGA, P<0.05), and 5 ($F_{2,14}$=4.467, P<0.05; *post hoc* comparisons: CON *vs.* DGA, P<0.01; PAE *vs.* DGA, P<0.05).

Fig. 6B (a) and B (b) represent the slice view of dendritic segments in Fig. 6A (a) (basal dendrites) and A (b) (apical dendrites), respectively. Visually, the differences in the dendritic morphology and density can be found between the groups. One-way ANOVA revealed the significant differences of dendritic spine density between the groups detected in both basal dendrites ($F_{2,14}$=9.948, P<0.01) and apical dendrites ($F_{2,14}$=4.461, P<0.05). *Post hoc* comparisons indicated that in the basal and apical dendrites, *D*-galactose and aluminum resulted in a remarkable decrease of the spine density, which can be relieved by treatment with paeonol in basal dendrites (Fig. 6C).

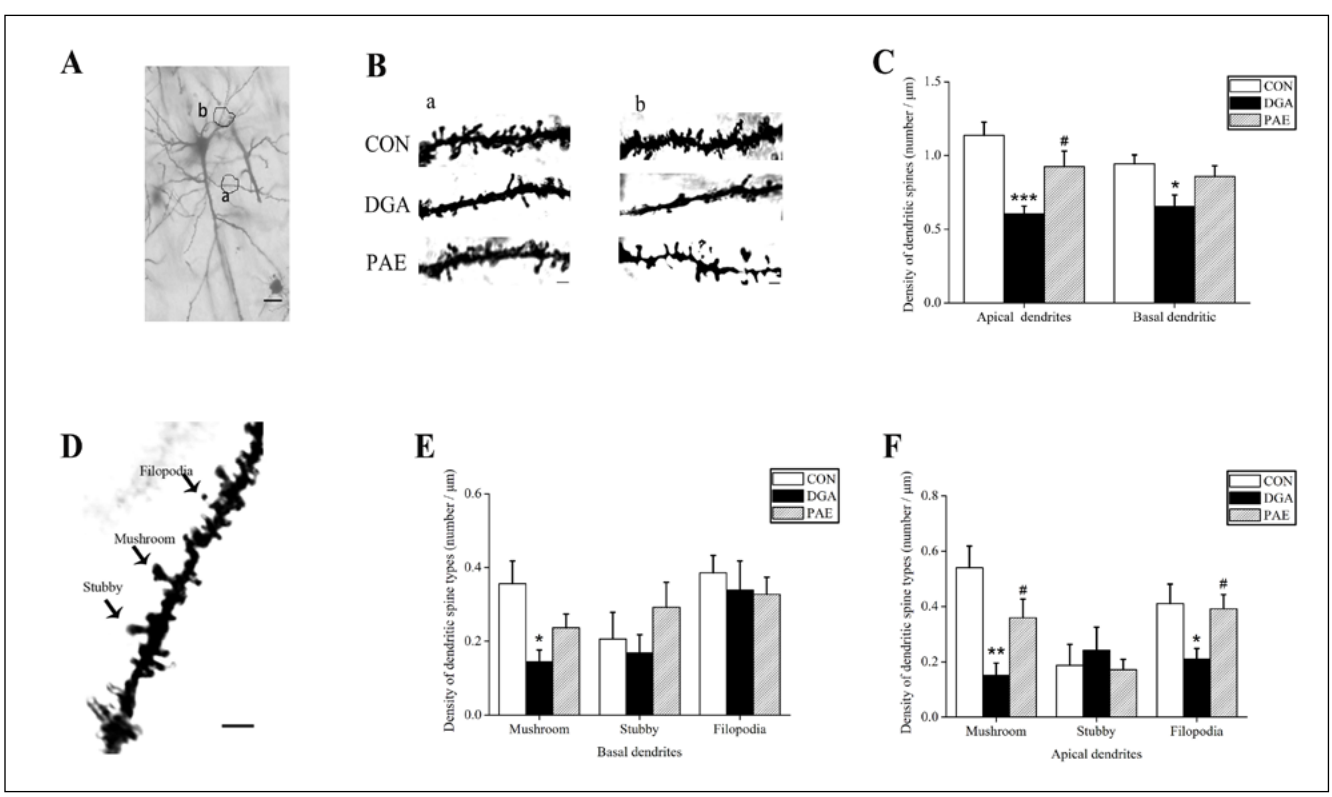

Fig. 6. Effects of paeonolon the density and type of dendritic spines in frontal cortex. (A) Pyramidal neurons in the frontal cortexlayer IIIstained by Golgi-Cox (scale: 20 μm). (B) Slice view acquired by Laser scanning confocal microscope (FV1000, 60×6 for objective magnification) at the apical (left column) and basal (right column) dendritic segments stained by Golgi-Cox method in frontal cortex. Paeonol treatment for 6 weeks significantly increased the dendritic spine density in apical dendrites but not in basal dendrites (C). (D) Types of dendritic spines (scale: 2 μm). In basal dendrites, adifference between CON and DGA was only found in the mushroom-type dendritic spines (E). However, in the apical dendrites, significant differences between groups existed in the mushroom-and filopodia-type spines (F). Data expressed as the means ± SEM. **P*<0.05, ***P*<0.01, ****P*<0.001 *versus* CON; #*P*<0.05 *versus* DGA.

In this study, according to the morphology of dendritic spines, they were divided into three types, mushroom, stubby and filopodia (Fig. 6D). In the basal dendrites, only mushroom-type dendritic spines existed differences between groups ($F_{2,14}$=5.383, P<0.05). *Post hoc* comparisons only showed a significant difference between CON and DGA (P<0.05), not between CON and PAE (P>0.05) or between PAE and DGA (P>0.05) (Fig. 6E). However, in the apical dendrites, significant differences between groups were observed in the types of mushroom ($F_{2,14}$=8.901, P<0.01) and filopodia ($F_{2,14}$=4.132, P<0.05). *Post hoc* comparisons manifested that paeonol treatment markedly attenuated *D*-galactose and aluminum-induced decline in the density of mushroom-type spines (CON *vs.* DGA, P<0.01; PAE *vs.* DGA, P<0.05) and filopodia-type spines (CON *vs.* DGA, P<0.05; PAE *vs.* DGA, P<0.05). Interestingly, there were no differences in the percentage of any types of dendritic spine found between the groups either in the basal dendrites or in the apical dendrites.

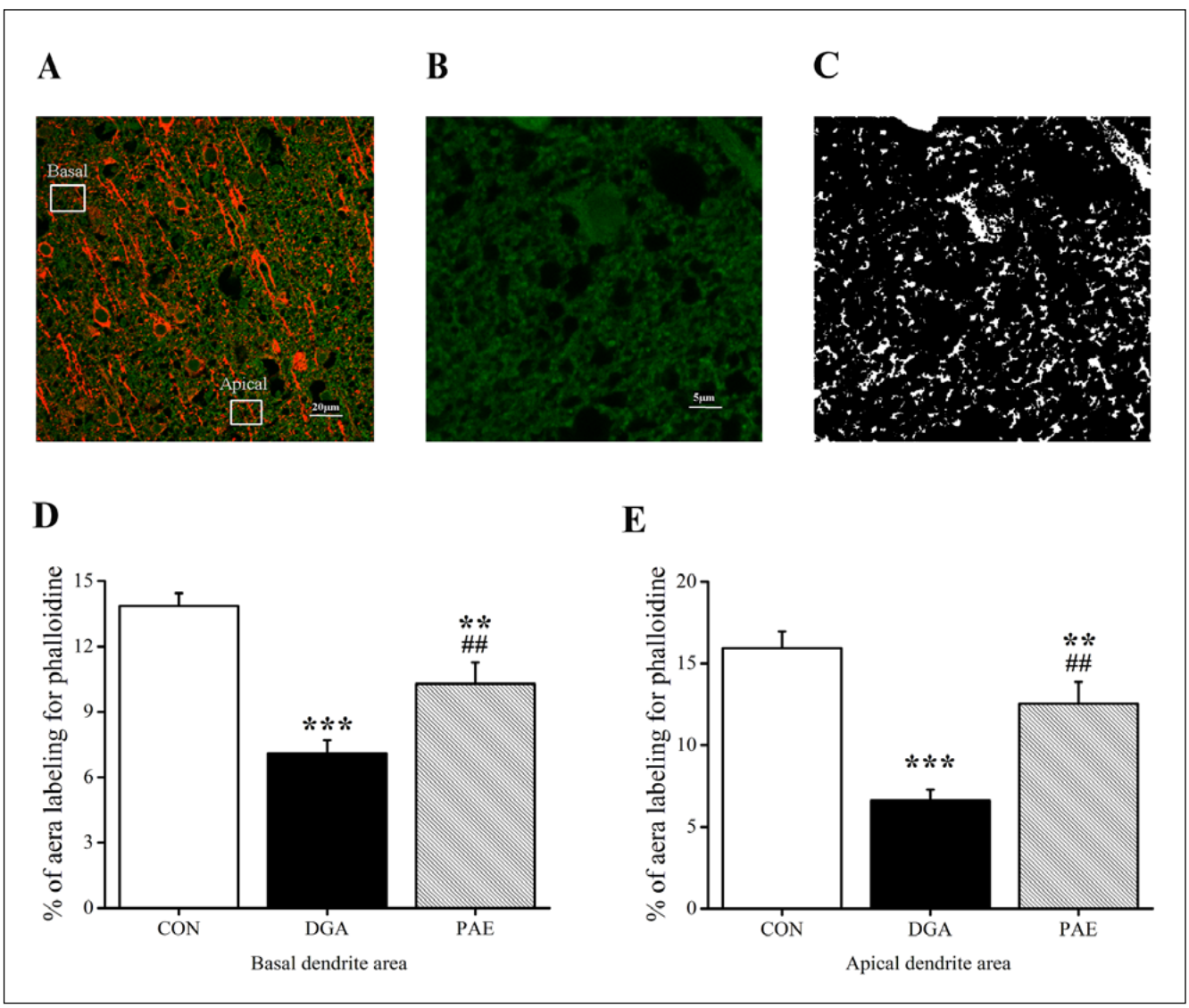

Fig. 7. Effects of Paeonol on F-actin density labeled by phalloidin staining in the frontal cortex. (A) A schematic diagram of the statistics area in the frontal cortex. MAP2 immunoreactivity (red) was used to distinguish the different areas (basal dendrite area and apical dendrite area) in the frontal cortex. (B) Magnification of the statistics area in a single channel of 488 nm (OLYMPUS FV1000). (C) Image of (B) was processed using ImageJ software. The background was subtracted with a rolling value of 15, converted to 8-bit deep images and binarized using a determined threshold value (reduce noise 5, particles 2-~). Statistical analysis for the percentage of phalloidin immunopositive area in basal dendrite area or apical dendrite area was expressed in (D) and (E), respectively. Data expressed as the means ± SEM (n=4~5). Scale bar in (A) represents 20 μm and in (B) represents 5 μm. **P<0.01, ***P<0.001 *versus* CON; ##P<0.05 *versus* DGA.

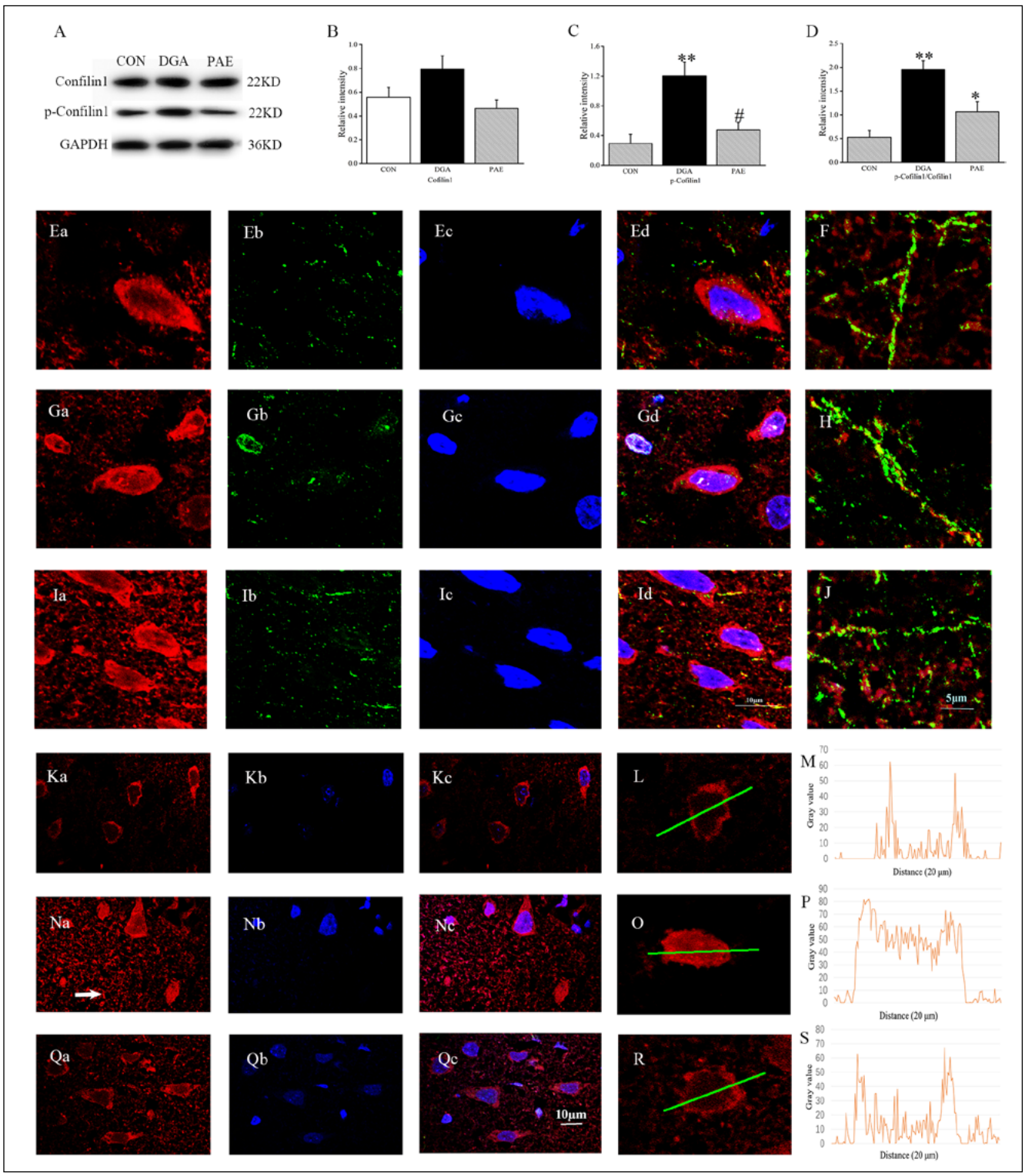

Fig. 8. Effects of paeonol on cofilin1 and p-cofilin1-immunoreactivity and their levels in frontal cortex. (A) Western blotting for cofilin1 and p-cofilin1 on Ser 3 in CON, DGA, and PAE. Paeonol downregulated the p-cofilin1 expression (C) and p-cofilin1/cofilin1 ratio (D), but did not affect the cofilin1 levels (B). Immunofluorescence labels of cofilin1 (red, excitation wavelength 543/emission wavelength bp560-615), p-cofilin1 (green excitation wave length 488/emission wave length bp500-530) and nucleus (blue, excitation wave length 458/emission wave length bp400-461) in frontal cortex (CON: E, F, K, L, and M; DGA: G, H, N, O, and P; PEA: I, J, Q, R, and S). The cells in (L), (O), and (R) are from (K), (N), and (Q), respectively. The fluorescence density curves of the single cell in (M), (P), and (S) were shown by the lines in (L), (O), and (R), respectively. White arrow in (Na) indicates the cofilin1-labeled dendrite similar to the "rod". Data expressed as the means ± SEM (n=3). Scale bars in (Id) and (Qc) represent 10 μm and in (J) represent 5 μm. **P*<0.05, ***P*<0.01 *versus* CON; #*P*<0.05 *versus* DGA.

Paeonol upregulated D-galactose and aluminum-induced decline of fibrillar actin in the frontal cortex

Actin filaments of ~200 nm diameter, which can be specifically labeled by phalloidin, constitute the dendritic spine cytoskeleton (Frost et al., 2010) and govern dendritic spine physiology by fibrillar actin (F-actin) nonequilibrium assembly and disassembly (Spence and Soderling, 2015). As shown in Fig. 7A, the rectangles represent the basal dendritic area and the apical dendrite area where the density of the actin filaments will be counted, respectively. One-way ANOVA indicated that both in the basal dendritic area ($F_{2,14}$=20.324, P<0.001) and the apical dendrite area ($F_{2,14}$=20.907, P<0.001), prominent differences in the density of actin filaments occurred between the groups. Treatment with paeonol significantly relieved *D*-galactose and aluminum-induced decline in the density of the actin filaments in the basal dendritic area (CON *vs.* DGA, P<0.001; PAE *vs.* CON, P<0.01; PAE *vs.* DGA, P<0.01) (Fig. 7D) as well as the apical dendrite area (CON *vs.* DGA, P<0.001; PAE *vs.* CON, P<0.01; PAE *vs.* DGA, P<0.01) (Fig. 7E).

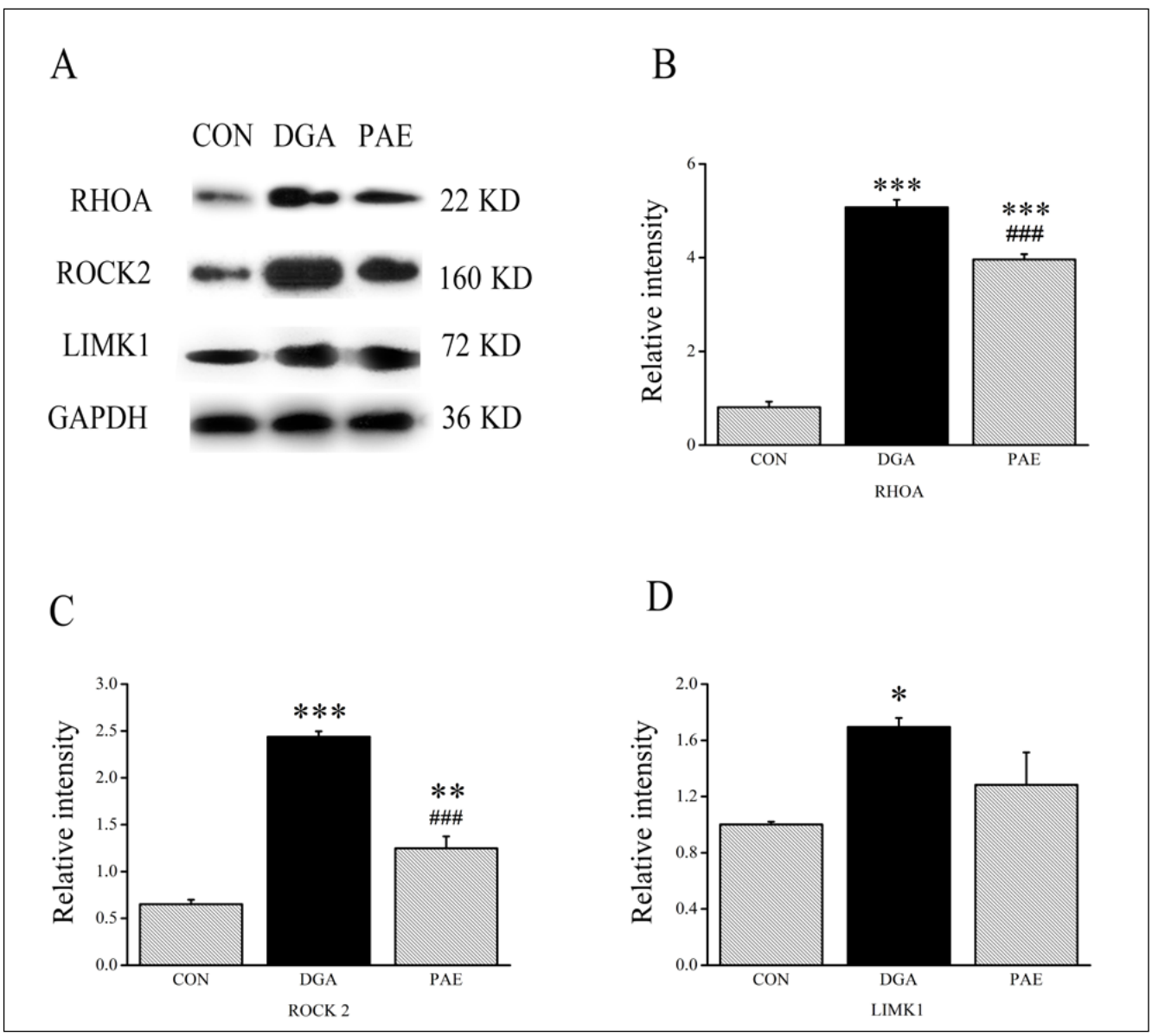

Fig. 9. Effects of paeonol on the levels of RhoA, Rock2, and Limk1. (A) Western blot bands of the frontal cortex tissues determined with RhoA, Rock2, and Limk1 antibodies in CON (left column), DGA (middle column), and PAE (right column). GAPDH (36 KD) is an internal reference. Treatment with paeonol (50 mg/kg, i.p.) for 6 weeks significantly alleviated *D*-gal and AlCl3-induced upregulation of RhoA (B) and Rock2 (C), as well as tended to significantly reduce the expression levels of Limk1 (D). Data expressed as the means ± SEM (n=3). *P<0.05, **P<0.01, ***P<0.001 *versus* CON; ###P<0.001 *versus* DGA.

Paeonol attenuated D-galactose and aluminum-induced alterations of cofilin1 in activity and redistribution in the frontal cortex

Cofilin1 as one of the best known regulators of actin remodeling (Pollard and Borisy, 2003; Bernstein and Bamburg, 2010), can be activated by dephosphorylation on Ser3 (Yang et al., 1998; Jose Javier et al., 2013) or release from membrane proteins (Shankar et al., 2007). Local excess inactivation or activation of cofilin1 may generate dendritic spine loss and dendrite atrophy (Van Troys et al., 2008; Bernstein and Bamburg, 2010). Therefore, in this study, we assessed the effects of paeonol on cofilin1 expression levels, activity, and redistribution in the frontal cortex.

Western blotting showed that *D*-galactose and aluminum did not change the cofilin1 expression levels ($F_{2,11}$=1.510, P>0.05), but did significantly increase p-cofilin1 levels ($F_{2,11}$=11.621, P<0.01) and p-cofilin1/cofilin1 ratio ($F_{2,11}$=14.639, P<0.01), these increases of which can be attenuated by paeonol treatment (p-cofilin1 and p-cofilin1/cofilin1 ratio: CON *vs.* DGA, P<0.01; PAE *vs.* DGA, P<0.05) (Fig. 8C and 8D).

Immunofluorescence revealed that cofilin1 immunoreactivity mainly distributed in the inner peri-membrane and neuronal processes, and p-cofilin1 was primarily found in the neuronal processes, in CON (Fig. 8E and 8F). In DGA, the distribution of cofilin1 translocated from the peri-membrane into the cytoplasm and nucleus, and p-cofilin1 prevailingly distributed in the nuclei and neuronal processes (Fig. 8G and 8H). Paeonol evidently relieved *D*-galactose and aluminum-induced increased distribution of p-cofilin1 in the nucleus and neuronal processes (Fig. 8I-J), and of cofilin1 in the cytoplasm and nucleus (Fig. 8K-S). Some cells with high immunopositive cofilin1 or p-cofilin1 in the nucleus and some cells colocalized with cofilin1 and p-cofilin1 in the nucleus (Fig. 8G) were mainly observed in DGA, and were occasionally found in CON or PAE.

Paeonol relieved D-galactose and aluminum-induced changes in RhoA, Rock2 and Limk1 levels in the frontal cortex

Activation of Rho/Rock2/Limk1 pathway promotes the phosphorylation of cofilin1 (Bravo-Cordero et al., 2013). So, we examined the effects of paeonol on the expression of these signal molecules by western blotting. The significant differences between groups were found in these signal molecules, including RhoA ($F_{2,8}$=260.230, P<0.001), Rock2 ($F_{2,8}$=113.402, P<0.001), and Limk1 ($F_{2,8}$=6.301, P<0.05). *Post hoc* comparisons displayed that *D*-galactose and aluminum caused a significant upregulation in the expression levels of RhoA (CON *vs.* DGA, P<0.001) (Fig. 9B), Rock2 (CON *vs.* DGA, P<0.001) (Fig. 9C), and Limk1 (CON *vs.* DGA, P<0.05) (Fig. 9D), these of which can be attenuated by treatment with paeonol (RhoA: PAE *vs.* DGA, P<0.001; Rock2: PAE *vs.* DGA, P<0.01; Limk1: PAE *vs.* DGA, P=0.081) (Fig. 9B-D).

DISCUSSION

In the present study, we found that paeonol attenuated *D*-galactose and aluminum-induced behavioral dysfunction and AD-like pathological alterations in the frontal cortex. Accompanied by these changes were the alterations in the dendrite and dendritic spine densities as well as actin filaments. In addition, the activity and intracellular distribution of cofilin1 and the molecules of the signaling pathway that regulate cofilin1 phosphorylation have also changed. Our data suggests that paeonol may be through reducing Aβ levels to alleviate the loss of fibrillar actin and dendrites and dendritic spines *via* the Rho/Rock2/Limk1/cofilin1 signaling pathway in the frontal cortex, and ultimately improving AD-like behavior.

AD is characterized as either familial early-onset (EOAD; onset<65 years) or sporadic late-onset (sAD; onset > 65 years) (Drummond and Wisniewski, 2017). sAD afflicts > 95% of patients with AD (Bertram and Tanzi, 2012; Dong et al., 2014; Guerreiro and Hardy, 2014; Karch et al., 2014). It has been proposed that the combined effect of multiple factors is the most likely cause of AD formation, especially for sAD (Farrer et al., 1997; Qiu et al., 2004; Seripa et al., 2009; Wyss-Coray and Rogers, 2012; Orsucci et al., 2013; Solomon et al., 2014). In AD-related research, it is essential to develop appropriate animal models for validly evaluating the pathological processes, which are usually difficult to perform in patients (Van Dam and De Deyn, 2011). Currently, there are multiple categories of animal models used for AD-related research, and each animal model on AD-related research has its own advantages and limitations (Van Dam and De Deyn, 2011). However, the presence of both pathological features, Aβ and hyperphosphorylated-tau, is important to replicate the toxicity that occurs in human AD (Prins et al., 2010). Crosstalk between Aβ and tau can significantly increase their toxicity (Drummond and Wisniewski, 2017), leading to a decline in memory and visuo-spatial skills, as well as emotional dysfunction such as depression and anxiety (Lyketsos et al., 2011; Ameen-Ali et al., 2017; Götz et al., 2018). These are clsosely related with the damage in certain brain regions including the frontal cortex (Lyketsos et al., 2011; Götz et al., 2018). In this study, *D*-galactose and aluminum-induced animal model produced the

classical AD-like pathological features and behavioral performances, these of which can be significantly attenuated by treatment with paeonol.

A large amount of evidence has shown that synaptic loss is the best pathologic correlate of cognitive dysfunction in AD (Forner et al., 2017). Dendritic spines that protrude from the main dendritic shaft form more than 90% of excitatory synapses (Leuner and Gould, 2010), and synapse strength and activity are inseparably linked to spine morphology (Yasunori and Majewska, 2005). In the early 1990s, synapse and dendritic spine loss has been already observed by electron microscopy and densitometry of immunostained synaptic proteins in several brain areas of AD, including the frontal cortex, temporal cortex, and dentate gyrus of the hippocampus (DeKosky and Scheff, 1990; DeKosky et al., 1996; Terry et al., 2010). Since then, a series of similar results have been reported. In aged Tg2576 mice cortical neurons, spine elimination increases, and spine stability are markedly impaired leading to loss of synaptic structural integrity (Spires-Jones et al., 2007). In apolipoprotein E (APOE, the strongest genetic risk factor for sporadic AD) targeted replacement (TR) mice, the APOE4 TR mice have significantly reduced spine density and shortened spines in the cortex neurons compared with APOE3 TR mice and APOE2 TR mice (Dumanis et al., 2009). In transgenic mice expressing human tau (htau), a shift in spine morphology with fewer mushroom and more thin spines in both apical and basal dendrites of layer III pyramidal neurons from the prefrontal cortex occurs as a function of htau accumulation, and there is an overall decrease in volume of spines from 3 to 12 months (Dickstein et al., 2010). In 5xFAD mice, a significant loss of spines on basal dendrites is found in the somatosensory and prefrontal cortices, but not in the hippocampus (Crowe and Ellis-Davies, 2014). In human, spine density within layer II and III pyramidal neuron dendrites in Brodmann area 46 dorsolateral prefrontal cortex is similar among control and CAD cases (cognitively normal individuals with high AD pathology) but is reduced significantly in AD; thin and mushroom spines are reduced significantly in AD compared to CAD brains (Boros et al., 2017). Even at the end of AD, quantitative analysis indicates that more close correlation of postmortem cytopathology with premortem cognitive deficits is synapse and dendritic spine loss, rather than the numbers of plaques or tangles, degree of neuronal perikaryal loss, or extent of cortical gliosis (Selkoe, 2002; Wu et al., 2010). Similarly, our results showed that in frontal cortex, paeonol significantly relieved *D*-galactose and aluminum-induced reduction in the dendritic length and branches and dendritic spine density, especially the mushroom- and filopodia-type spines, suggesting that attenuation of spine loss by paeonol is mainly through reducing the loss of functional mature dendritic spines (mushroom) and increasing the production of new dendritic spines (filopodia).

It is well demonstrated that dendritic spine remodeling depends on the remodeling of cytoskeleton protein actin, which provides integrity for dendritic spines and organizes signaling machinery (Dillon and Goda, 2005; Schubert and Dotti, 2007; Bernstein and Bamburg, 2010; Sala and Segal, 2014; Maiti et al., 2015). Continuous actin polymerization into F-actin and depolymerization into globular actin (G-actin) are of major importance for the dynamic behavior of dendritic spines, contributing to their support, remodeling, and synaptic plasticity (Zhang and Benson, 2001; Star et al., 2002; Okamoto et al., 2004; Honkura et al., 2008). Therefore, it is well logical for our findings that the consistent alterations with dendrites and dendritic spines in the frontal cortex are F-actin specifically labeled by phalloidin.

In addition, actin also translocate into the nucleus (de Lanerolle and Serebryannyy, 2011; Dopie et al., 2012), in which nuclear actin is important in regulating gene accessibility, transcription, and post-transcriptional regulation (de Lanerolle and Serebryannyy, 2011). Studies have revealed that actin filament non-equilibrium assembly and disassembly is regulated by many factors including the actin-depolymerizing factor (ADF)/cofilin family that consists of three highly similar paralogs: ADF, cofilin1 (non-muscle cofilin), cofilin2 (muscle cofilin) (Bamburg and Wiggan, 2002; Bernstein and Bamburg, 2010). ADF/cofilin family has multiple functions and is called a functional node in cell biology (Bernstein and Bamburg, 2010). Cofilin1 is the most widely expressed member of the ADF/cofilin family, especially in mammal neurons (Bernstein and Bamburg, 2010), and is also considered as the most conserved and essential protein accelerating actin filament disassembly in cells (Vepsäläinen et al., 2013). Inhibition of cofilin1 is consequently lethal at the embryonic stage (Andrianantoandro and Pollard, 2006; Bernstein and Bamburg, 2010). Cofilin1 can be activated in a variety of ways, including dephosphorylation on its Ser3 and release of cofilin1 from membrane protein binding (Bernstein and Bamburg, 2010). However, misregulation of ADF/cofilin activity is linked to several pathologies (Yamaguchi and Condeelis, 2007; Wioland et al., 2017). Local excess activation or inactivation of cofilin may lead to dendritic spine loss and dendrite atrophy (Van Troys et al., 2008; Bernstein and Bamburg, 2010). In this study, we found that *D*-galactose and aluminum significantly elevated the p-cofilin1 levels, increased the distribution of cofilin1 translocating from the peri-membrane into the cytoplasm and nucleus, and/or aggrandized the p-cofilin1 prevailingly distrib-

uting in the nuclei and neuronal processes (Fig. 8 G and H), these of which can be attenuated by treatment with paeonol. Our results suggest that the prevention of dendrite and dendritic spine loss by paeonol may be through regulating the activity of cofilin1 by affecting its local distribution in cells, and/or regulating the transcription of related genes in the nucleus *via* cofilin1 phosphorylation.

Early evidence has indicated that increased soluble Aβ oligomers (also known as Aβ-derived diffusible ligands, ADDLs), especially the Aβ oligomers at 56 kDa and pI 5.6, can induce synaptic loss in neurons *in vitro* and *in vivo* (Yuesong et al., 2003; Lacor et al., 2007; Ittner and Gotz, 2011), and highly correlate with impaired behaviors in AD (Sylvain et al., 2006). *In vitro*, soluble Aβ disrupts actin and microtubule dynamics *via* activation of RhoA and inhibition of histone deacetylase 6 (HDAC6) in cultured neurons (Tsushima et al., 2015). Aβ activates the RhoA GTPase by binding to p75NTR, and the inactivation of RhoA GTPase can protect cultured neurons against the noxious effects of Aβ (Chacon et al., 2011)2011. In APP Tg mice, RhoA expression levels were increased in dystrophic neurites (Gema et al., 2009). Knockdown or pharmacologic inhibition of ROCK2, the downstream kinase of RhoA, decreased Aβ levels in the5XFAD AD mouse (Herskowitz et al., 2013). LIMK1 (LIM motif-containing protein kinase 1 is a serine/threonine kinase protein, also the downstream kinase of ROCK2, and can phosphorylate cofilin1 at Ser 3 forming inactivated p-cofilin1 (Scott et al., 2010; Bravo-Cordero et al., 2011) to regulate the neuronal morphology (Bernard, 2007). LIMK1 activation may play a key role in AD pathology (Heredia et al., 2006). The *limk1* gene knockout mouse exhibits significant abnormalities in the morphology of dendritic spines and neurite growth cones and synaptic functions (Meng et al., 2002). Pharmacologic inhibition of LIMK1 provides dendritic spine resilience against β-amyloid (Henderson et al., 2019). These data indicate a RhoA-ROCK2-LIMK1-cofilin1 pathway really existed in the progress of AD. Our results that paeonol relieved *D*-galactose and aluminum-induced elevation of RhoA, ROCK2, and LIMK1 levels suggest this pathway involved in the protective effects of paeonol on dendrites and dendritic spines.

Additionally, studies reveal that LIMKs are inactivated by SSH-mediated dephosphorylation (Soosairajah et al., 2014), and specific inhibitors for PI3K inhibite SSH1L activation (Nishita et al., 2004), indicating a negative relationship in the activity between LIMK1 and PI3K and/or SSH1. So, we examined the effects of paeonol on PI3K and SSH1 levels. Our results showed that paeonol remarkably relieved *D*-galactose and aluminum-induced downregulation of PI3K (Fig. 10B) and SSH1 (Fig. 10C) levels in the frontal cortex.

In conclusion, we have identified that paeonol has a protective role against dendrite atrophy and dendritic spine loss in frontal cortex. Furthermore, the protective efficacy is, at least in part, through the RhoA-ROCK2-LIMK1 pathway to regulate the cofilin1 activity and reduce the dendrite atrophy and dendritic spine loss, eventually attenuate the AD-like behavioral abnormalities.

ACKNOWLEDGMENTS

We thank Mr. Hao Yan and Ms. Xiao-Yan Ma for help with the confocal photomicrographs. This work was supported by the National Natural Science Foundation of China (No. 30470537), the Natural Science Foundation of the Department of Education, Anhui Province

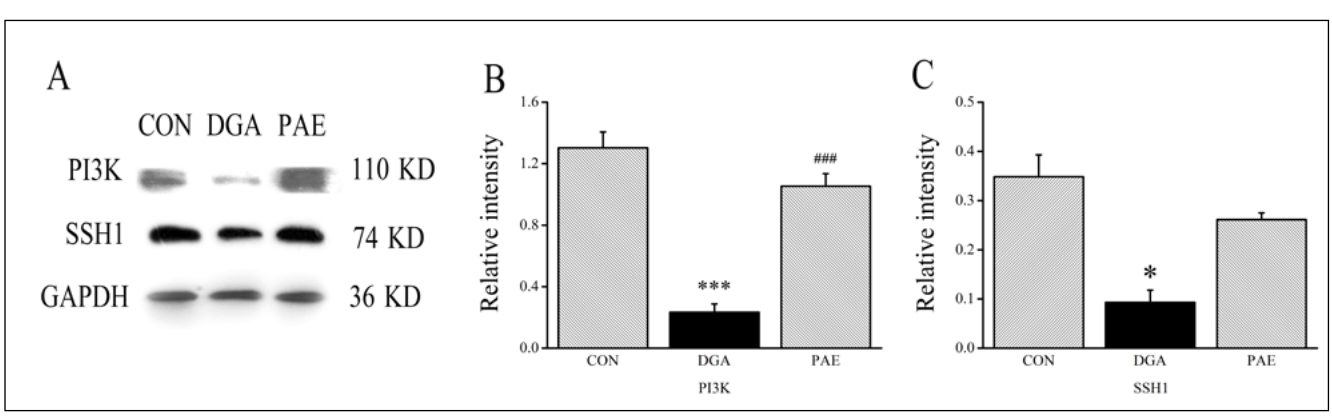

Fig. 10. Effects of paeonol on PI3K and SSH1 levels. (A) Western blot bands of the frontal cortex tissues determined by PI3K and SSH1 antibodies in CON (left column), DGA (middle column), and PAE (right column). GAPDH (36 KD) is an internal reference. Treatment with paeonol (50 mg/kg, i.p.) for 6 weeks significantly alleviated *D*-gal and AlCl3-induced downregulation of PI3K (B) and SSH1 (C). Data expressed as the means ± SEM (n=3). **P*<0.05, 1047, ****P*<0.001 *versus* CON; ###*P*<0.001 *versus* DGA.

(ZD2008006-1), the Innovation Team of Scientific Research Platform in Anhui Universities, Anhui Provincial Key Lab of the Conservation and Exploitation of Biological Resources, the Provincial Key Laboratory of Biotic Environment and Ecological Safety in Anhui and the Key Laboratory of Genetic Diseases and Health Biomedicine of Anhui Province.

REFERENCES

Alzheimer's Association (2019) Alzheimer's disease facts and figures, Alzheimer's Dementia, pp. 321–387.

Ameen-Ali KE, Wharton, SB, Simpson, JE, Heath PR, Sharp P, Berwick J (2017) Neuropathology and behavioural features of transgenic murine models of Alzheimer's disease. Neuropathol Appl Neurobiol 43: 553–570.

Anderson RM, Hadjichrysanthou C, Evans S, Wong MM (2017) Why do so many clinical trials of therapies for Alzheimer's disease fail? Lancet 390: 2327–2329.

Andrianantoandro E, Pollard, TD (2006) Mechanism of actin filament turnover by severing and nucleation at different concentrations of ADF/cofilin. Mol Cell 24: 13–23.

Bamburg JR, Wiggan OP (2002) ADF/cofilin and actin dynamics in disease. Trends Cell Biol 12: 598–605.

Bateman RJ, Chengjie X, Benzinger TLS, Fagan AM, Alison G, Fox NC, Marcus DS, Cairns NJ, Xianyun X, Blazey TM (2012) Clinical and biomarker changes in dominantly inherited Alzheimer's disease. N Eng J Med 367: 795–804.

Bernard O (2007) Lim kinases, regulators of actin dynamics. Int J Biochem Cell Biol 39: 1071–1076.

Bernstein BW, Bamburg, JR (2010) ADF/cofilin: a functional node in cell biology. Trends Cell Biol 20: 187–195.

Bertram L, Tanzi RE (2012) The genetics of Alzheimer's disease. Prog Mol Biol Transl Sci 107: 79–100.

Boros BD, Greathouse KM, Gentry EG, Curtis KA, Birchall EL, Gearing M, Herskowitz JH (2017) Dendritic spines provide cognitive resilience against Alzheimer's disease. Ann Neurol 82: 602–614.

Bravo-Cordero JJ, Magalhaes MA, Eddy RJ, Hodgson L, Condeelis J (2013) Functions of cofilin in cell locomotion and invasion. Nat Rev Mol Cell Biol 14: 405–415.

Bravo-Cordero JJ, Oser M, Chen X, Eddy R, Hodgson L, Condeelis J (2011) A novel spatiotemporal RhoC activation pathway locally regulates cofilin activity at invadopodia. Curr Biol 21: 635–644.

Bringas ME, Carvajal-Flores FN, Lopez-Ramirez TA, Atzori M, Flores G (2013) Rearrangement of the dendritic morphology in limbic regions and altered exploratory behavior in a rat model of autism spectrum disorder. Neuroscience 241: 170–187.

Chacon PJ, Garcia-Mejias R, Rodriguez-Tebar A (2011) Inhibition of RhoA GTPase and the subsequent activation of PTP1B protects cultured hippocampal neurons against amyloid beta toxicity. Mol Neurodegener 6: 14.

Chiroma SM, Baharuldin MTH, Taib M, Norma C, Amom Z, Jagadeesan S, Ilham Adenan M, Mahdi O, Moklas MAM (2019) Centella asiatica Protects d-Galactose/$AlCl_3$ Mediated Alzheimer's Disease-Like Rats via PP2A/GSK-3β Signaling Pathway in Their Hippocampus. Inte J Mol Sci 20: 1871.

Crowe SE, Ellis-Davies GC (2014) Spine pruning in 5xFAD mice starts on basal dendrites of layer 5 pyramidal neurons. Brain Struct Funct 219: 571–580.

DeKosky ST, Scheff SW (1990) Synapse loss in frontal cortex biopsies in Alzheimer's disease: correlation with cognitive severity. Annals Neurol 27: 457–464.

DeKosky ST, Scheff SW, Styren SD (1996) Structural correlates of cognition in dementia: quantification and assessment of synapse change. Neurodegeneration 5: 417–421.

de Lanerolle P, Serebryannyy L (2011) Nuclear actin and myosins: life without filaments. Nature Cell Biol 13: 1282–1288.

Dickstein DL, Brautigam H, Stockton SD Jr, Schmeidler J, Hof PR (2010) Changes in dendritic complexity and spine morphology in transgenic mice expressing human wild-type tau. Brain Struct Funct 214: 161–179.

Dillon C, Goda Y (2005) The actin cytoskeleton: Integrating form and function at the synapse. Ann Review Neurosci 28: 25–55.

Dong HK, Yeo SH, Park JM, Ji YC, Lee TH, Park SY, Ock MS, Eo J, Kim HS, Cha HJ (2014) Genetic markers for diagnosis and pathogenesis of Alzheimer's disease. Gene 545: 185–193.

Doody RS, Rema R, Martin F, Takeshi I, Bruno V, Steven J, Karl K, Feng H, Xiaoying S, Thomas RG (2013) A phase 3 trial of semagacestat for treatment of Alzheimer's disease. N Eng J Med 369: 341.

Dopie J, Skarp KP, Rajakylä EK, Tanhuanpää K, Vartiainen MK (2012) Active maintenance of nuclear actin by importin 9 supports transcription. Proc Natl Acad Sci 109: E544–552.

Drummond E, Wisniewski T (2017) Alzheimer's disease: experimental models and reality. Acta Neuropathol 133: 155–175.

Dumanis SB, Tesoriero JA, Babus LW, Nguyen MT, Trotter JH, Ladu MJ, Weeber EJ, Turner RS, Xu B, Rebeck GW, Hoe HS (2009) ApoE4 decreases spine density and dendritic complexity in cortical neurons in vivo. J Neurosci 29: 15317–15322.

Egan MF, Kost J, Tariot PN, Aisen PS, Cummings JL, Vellas B, Sur C, Mukai Y, Voss T, Furtek C (2018) Randomized trial of verubecestat for mild-to-moderate Alzheimer's disease. N Engl J Med 378: 1691–1703.

Farrer LA, Cupples LA, Haines JL, Hyman B, Kukull WA, Mayeux R, Myers RH, Pericak-Vance MA, Risch N, van Duijn CM (1997) Effects of age sex and ethnicity on the association between apolipoprotein E genotype and Alzheimer disease. A meta-analysis. APOE and Alzheimer Disease Meta Analysis Consortium. JAMA 278: 1349–1356.

Fernando GI, Frances P, Yong J, Henrieta S, Jing Y, Yanjie S, Feng-Xia L, Regina K, Richard K, Pankaj M (2010) Immunomodulation targeting abnormal protein conformation reduces pathology in a mouse model of Alzheimer's disease. Plos One 5 e13391.

Flores G, Alquicer G, Silva-Gomez AB, Zaldivar G, Stewart J, Quirion R, Srivastava LK (2005) Alterations in dendritic morphology of prefrontal cortical and nucleus accumbens neurons in post-pubertal rats after neonatal excitotoxic lesions of the ventral hippocampus. Neuroscience 133: 463–470.

Forner S, Baglietto-Vargas D, Martini AC, Trujillo-Estrada L, LaFerla FM (2017) Synaptic impairment in Alzheimer's disease: A dysregulated symphony. Trends Neurosci 40: 347–357.

Foster Olive M, Del Franco AP, Gipson CD (2018) Diolistic labeling and analysis of dendritic spines. Methods Mol Biol 1727: 179–200.

Frost NA, Hari S, Huihui K, Eric B, Blanpied TA (2010) Single-molecule discrimination of discrete perisynaptic and distributed sites of actin filament assembly within dendritic spines. Neuron 67: 86–99.

Gema H, María Antonia B, Pilar GR, Asunción M, Agustina G, Juan H, Silvia F, Gabriel S, Isidre F, Elena, G (2009) Altered distribution of RhoA in Alzheimer's disease and AbetaPP overexpressing mice. J Alzheimers Dis 19: 37–56.

Gordon BA, Blazey TM, Su Y, Hari-Raj A, Dincer A, Flores S, Christensen J, Mcdade E, Wang G, Xiong C (2018) Spatial patterns of neuroimaging biomarker change in individuals from families with autosomal dominant Alzheimer's disease: a longitudinal study. Lancet Neurol 17: 241–250.

Götz J, Bodea LG, Goedert M (2018) Rodent models for Alzheimer disease. Nat Rev Neurosci 19: 583–598.

Grontvedt, GR, Schroder, TN, Sando, SB, White, L, Brathen, G, Doeller, CF (2018) Alzheimer's disease. Curr Biol 28: R645-R649.

Guerreiro R, Hardy J (2014) Genetics of Alzheimer's Disease. Neurotherapeutics 11: 732–737.

Hagen S, Boyd CS, Ruhi A, Spencer JPE, Duncan RF, Catherine RE, Enrique C (2003) c-Jun N-terminal kinase (JNK)-mediated modulation of brain mitochondria function: new target proteins for JNK signalling in mitochondrion-dependent apoptosis. Biochem J 372: 359–369.

Han F, Zhuang TT, Chen JJ, Zhu XL, Cai YF, Lu YP (2017) Novel derivative of Paeonol, Paeononlsilatie sodium, alleviates behavioral damage and hippocampal dendritic injury in Alzheimer's disease concurrent with cofilin1/phosphorylated-cofilin1 and RAC1/CDC42 alterations in rats. PLoS One 12: e0185102.

Heiko B, Thal DR, Estifanos G, Kelly DT (2011) Stages of the pathologic process in Alzheimer disease: age categories from 1 to 100 years. J Neuropathol Exp Neurol 70: 960.

Henderson BW, Greathouse KM, Ramdas R, Walker CK, Rao TC, Bach SV, Curtis KA, Day JJ, Mattheyses AL, Herskowitz JH (2019) Pharmacologic inhibition of LIMK1 provides dendritic spine resilience against beta-amyloid. Sci Signal 12: eaaw9318.

Heredia L, Helguera P, Olmos SD, Kedikian G, Vigo FS, Laferla F, Staufenbiel M, Olmos JD, Busciglio J, Cáceres A (2006) Phosphorylation of actin-depolymerizing factor/cofilin by LIM-kinase mediates amyloid β-induced degeneration: a potential mechanism of neuronal dystrophy in Alzheimer's disease. J Neurosci 26: 6533–6542.

Herskowitz JH, Feng Y, Mattheyses AL, Hales CM, Higginbotham LA, Duong DM, Montine TJ, Troncoso JC, Thambisetty M, Seyfried NT, Levey AI, Lah JJ (2013) Pharmacologic inhibition of ROCK2 suppresses amyloid-beta production in an Alzheimer's disease mouse model. J Neurosci 33: 19086–19098.

Honkura N, Matsuzaki M, Noguchi J, Ellis-Davies,GCR, Kasai H (2008) The subspine organization of actin fibers regulates the structure and plasticity of dendritic spines. Neuron 57: 719–729.

Hu XY, Qin S, Lu YP, Ravid R, Swaab DF, Zhou JN (2003) Decreased estrogen receptor-alpha expression in hippocampal neurons in relation to hyperphosphorylated tau in Alzheimer patients. Acta Neuropathol 106: 213–220.

Hyman BT, Phelps CH, Beach TG, Bigio EH, Cairns NJ, Carrillo MC, Dickson DW, Duyckaerts C, Frosch MP, Masliah E (2012) National Institute on Aging–Alzheimer's Association guidelines for the neuropathologic assessment of Alzheimer's disease. Acta Neuropathol 123: 1–11.

Ishiguro K, Ando T, Maeda O, Hasegawa M, Kadomatsu K, Ohmiya N, Niwa Y, Xavier R, Goto H (2006) Paeonol attenuates TNBS-induced colitis by inhibiting NF-κB and STAT1 transactivation. Toxicol Appl Pharmacol 217: 35–42.

Ittner A, Ittner LM (2018) Dendritic Tau in Alzheimer's disease. Neuron 99: 13–27.

Ittner LM, Gotz J (2011) Amyloid-beta and tau – a toxic pas de deux in Alzheimer's disease. Nat Rev Neurosci 12: 65–72.

Jack CR, Lowe VJ, Weigand SD, Wiste HJ, Senjem ML, Knopman DS, Shiung MM, Gunter JL, Boeve BF, Kemp BJ (2009) Serial PIB and MRI in normal, mild cognitive impairment and Alzheimer's disease: implications for sequence of pathological events in Alzheimer's disease. Brain 132: 1355–1365.

Juan YC, Tsai WJ, Lin YL, Wang GJ, Cheng JJ, Yang HY, Hsu CY, Liu HK (2010) The novel anti-hyperglycemic effect of Paeoniae radix via the transcriptional suppression of phosphoenopyruvate carboxykinase (PEPCK). Phytomedicine 17: 626–634.

Karch CM, Cruchaga C, Goate AM (2014) Alzheimer's disease genetics: from the bench to the clinic. Neuron 83: 11–26.

Kolb B, Forgie M, Gibb R, Gorny G, Rowntree S (1998) Age, experience and the changing brain. Neurosci Biobehav Rev 22: 143–159.

Kubes P, Mehal WZ (2012) Sterile inflammation in the liver. Gastroenterology 143: 1158–1172.

Lacor PN, Buniel MC, Furlow PW, Clemente AS, Klein WL (2007) A Oligomer-induced aberrations in synapse composition, shape, and density provide a molecular basis for loss of connectivity in Alzheimer's disease. J Neurosci 27: 796–807.

Lau CH, Chan CM, Chan YW, Lau KM, Lau TW, Lam FC, Law WT, Che CT, Leung PC, Fung KP (2007) Pharmacological investigations of the anti-diabetic effect of Cortex Moutan and its active component paeonol. Phytomedicine 14: 778–784.

Lazcano Z, Solis O, Bringas ME, Limon D, Diaz A, Espinosa B, Garcia-Pelaez I, Flores G, Guevara J (2014) Unilateral injection of Abeta25–35 in the hippocampus reduces the number of dendritic spines in hyperglycemic rats. Synapse 68: 585–594.

Lesne SE, Sherman MA, Grant M, Kuskowski M, Schneider JA, Bennett DA, Ashe KH (2013) Brain amyloid-β oligomers in ageing and Alzheimers disease. Brain 136: 1383–1398.

Leuner B, Gould E (2010) Structural plasticity and hippocampal function. Ann Rev Psychol 61: 111–140.

Li C, Yang L, Wu H, Dai M (2018a) Paeonol inhibits oxidized low-density lipoprotein-induced vascular endothelial cells autophagy by upregulating the expression of miRNA-30a. Front Pharmacol 9: 95.

Li X, Huang X, Tang Y, Zhao F, Cao Y, Yin L, Li G (2018b) Assessing the Pharmacological and therapeutic efficacy of traditional chinese medicine Liangxue Tongyu prescription for intracerebral hemorrhagic stroke in neurological disease models. Front Pharmacol 9: 1169.

Lin B (2011) Polyphenols and neuroprotection against ischemia and neurodegeneration. Mini Rev Med Chem 11: 1222 -1238.

Liu MH, Lin AH, Ko HK, Perng DW, Lee TS, Kou YR (2017) Prevention of bleomycin-induced pulmonary inflammation and fibrosis in mice by paeonol. Front Physiol 8: 193.

Liu Y, Li C, Wu H, Xie X, Sun Y, Dai M (2018) Paeonol Attenuated inflammatory response of endothelial cells via stimulating monocytes-derived exosomal microRNA-223. Front Pharmacol 9: 1105.

Lu S, Han Y, Chu H, Kong L, Zhang A, Yan G, Sun H, Wang P, Wang X (2017) Characterizing serum metabolic alterations of Alzheimer's disease and intervention of Shengmai-San by ultra-performance liquid chromatography/electrospray ionization quadruple time-of-flight mass spectrometry. Food Func 8: 1660–1671.

Lyketsos CG, Carrillo MC, Ryan JM, Khachaturian AS, Trzepacz P, Amatniek J (2011) Neuropsychiatric symptoms in alzheimer's disease. Alzheimer's Dementia 7: 532–539.

Ma L, Chuang CC, Weng W, Zhao L, Zheng Y, Zhang J, Zuo L (2016) Paeonol Protects rat heart by improving regional blood perfusion during no-reflow. Front Physiol 7: 298.

Maiti P, Manna J, Ilavazhagan G, Rossignol J, Dunbar GL (2015) Molecular regulation of dendritic spine dynamics and their potential impact on synaptic plasticity and neurological diseases. Neurosci Biobehav Rev 59: 208–237.

Martinez-Tellez RI, Hernandez-Torres E, Gamboa C, Flores G (2009) Prenatal stress alters spine density and dendritic length of nucleus accumbens and hippocampus neurons in rat offspring. Synapse 63: 794–804.

Mavroudis IA, Fotiou DF, Manani MG, Njaou SN, Frangou D, Costa VG, Baloyannis SJ (2011) Dendritic pathology and spinal loss in the visual cortex in Alzheimer's disease: a Golgi study in pathology. Int J Neurosci 121: 347–354.

Meng Y, Yu Z, Tregoubov V, Janus C, Cruz L, Jackson M, Lu WY, Macdonald JF, Wang JY, Falls DL (2002) Abnormal Spine morphology and enhanced LTP in LIMK-1 knockout mice. Neuron 35: 121–133.

Morris R (1984) Developments of a water-maze procedure for studying spatial learning in the rat. J Neurosci Meth 11: 47–60.

Nishita M, Wang Y, Tomizawa C, Suzuki A, Niwa R, Uemura T, Mizuno K (2004) Phosphoinositide 3-kinase-mediated activation of cofilin phosphatase Slingshot and its role for insulin-induced membrane protrusion. J Biol Chem 279: 7193–7198.

Okamoto K, Nagai TA, Hayashi Y (2004) Rapid and persistent modulation of actin dynamics regulates postsynaptic reorganization underlying bidirectional plasticity. Nature Neuroscience 7: 1104–1112.

Orsucci D, Mancuso M, Ienco EC, Simoncini C, Siciliano G, Bonuccelli U (2013) Vascular factors and mitochondrial dysfunction: a central role in the pathogenesis of Alzheimer's disease. Curr Neurovascular Res 10: 76–80.

Paxinos G, Watson C (2006) The Rat Brain in Stereotaxic Coordinates. Sixth Edition.

Pellow S, Chopin P, File SE, Briley M (1985) Validation of open: closed arm entries in an elevated plus-maze as a measure of anxiety in the rat. J Neurosci Meth 14: 149–167.

Pollard TD, Borisy GG (2003) Cellular motility driven by assembly and disassembly of actin filaments. Cell 112: 453–465

Prins ND, Visser PJ, Scheltens P (2010) Can novel therapeutics halt the amyloid cascade? Alzheimers Res Ther 2: 5.

Qiu C, Kivipelto M, Aguero-Torres H, Winblad B, Fratiglioni L (2004) Risk and protective effects of the APOE gene towards Alzheimer's disease in the Kungsholmen project: variation by age and sex. J Neurol Neurosurg Psychiatry 75: 828–833.

Reiman EM, Quiroz YT, Fleisher AS, Chen K, Velez-Pardo C, Jimenez-Del--Rio M, Fagan AM, Shah AR, Alvarez S, Arbelaez A (2012) Brain imaging and fluid biomarker analysis in young adults at genetic risk for autosomal dominant Alzheimer's disease in the presenilin 1 E280A kindred: a case-control study. Lancet Neurol 11: 1048–1056.

Risher WC, Ustunkaya T, Singh Alvarado J, Eroglu C (2014) Rapid Golgi analysis method for efficient and unbiased classification of dendritic spines. PLoS One 9: e107591.

Sadowski MJ, Pankiewicz J, Scholtzova H, Mehta PD, Prelli F, Quartermain D, Wisniewski T (2006) Blocking the apolipoprotein E/amyloid-beta interaction as a potential therapeutic approach for Alzheimer's disease. Proc Nat Acad Sci USA 103: 18787–18792.

Sala C, Segal M (2014) Dendritic spines: the locus of structural and functional plasticity. Physiol Rev 94: 141–188.

Schubert V, Dotti CG (2007) Transmitting on actin: synaptic control of dendritic architecture. J Cell Science 120: 205–212.

Scott RW, Steven H, Diane C, Li A, Ireen K, June M, Elisabeth T, Grant W, Pierre M, Croft DR (2010) LIM kinases are required for invasive path generation by tumor and tumor-associated stromal cells. J Cell Biol 191: 169–185.

Sebastian V, Estil JB, Chen D, Schrott LM, Serrano PA (2013) Acute physiological stress promotes clustering of synaptic markers and alters spine morphology in the hippocampus. PloS One 8: e79077.

Selkoe DJ (2002) Alzheimer's disease is a synaptic failure. Science 298: 789–791.

Seripa D, Panza F, Franceschi M, D'Onofrio G, Solfrizzi V, Dallapiccola B, Pilotto A (2009) Non-apolipoprotein E and apolipoprotein E genetics of sporadic Alzheimer's disease. Ageing Res Rev 8: 214–236.

Shankar GM, Bloodgood BL, Matthew T, Walsh DM, Selkoe DJ, Sabatini BL (2007) Natural oligomers of the Alzheimer amyloid-beta protein induce reversible synapse loss by modulating an NMDA-type glutamate receptor-dependent signaling pathway. J Neurosci 27: 2866–2875.

Solomon A, Mangialasche F, Richard E, Andrieu S, Bennett DA, Breteler M, Fratiglioni L, Hooshmand B, Khachaturian AS, Schneider LS, Skoog I, Kivipelto M (2014) Advances in the prevention of Alzheimer's disease and dementia. J Intern Med 275: 229–250.

Soosairajah J, Maiti S, Wiggan O, Sarmiere P, Moussi N, Sarcevic B, Sampath R, Bamburg JR, Bernard O (2005) Interplay between components of a novel LIM kinase-slingshot phosphatase complex regulates cofilin. EMBO J 24: 473–486.

Spence EF, Soderling SH (2015) Actin out: regulation of the synaptic cytoskeleton. J Biol Chem 290: 28613–28622.

Spires-Jones TL, Meyer-Luehmann M, Osetek JD, Jones PB, Stern EA, Bacskai BJ, Hyman BT (2007) Impaired spine stability underlies plaque-related spine loss in an Alzheimer's disease mouse model. Am J Pathol 171: 1304–1311.

Star EN, Kwiatkowski DJ, Murthy VN (2002) Rapid turnover of actin in dendritic spines and its regulation by activity. Nature Neurosci 5: 239–246.

Sun ZZ, Chen ZB, Jiang H, Li LL, Li EG, Xu Y (2009) Alteration of Aβ metabolism-related molecules in predementia induced by $AlCl_3$ and D-galactose. Age 31: 277–284.

Sylvain L, Teng KM, Linda K, Rakez K, Glabe CG, Austin Y, Michela G, Ashe KH (2006) A specific amyloid-beta protein assembly in the brain impairs memory. Nature 440: 352–357.

Tang M, Ryman DC, McDade E, Jasielec MS, Buckles VD, Cairns NJ, Fagan AM, Goate A, Marcus DS, Xiong C, Allegri RF, Chhatwal JP, Danek A, Farlow MR, Fox NC, Ghetti B, Graff-Radford NR, Laske C, Martins RN, Masters CL, Mayeux RP, Ringman JM, Rossor MN, Salloway SP, Schofield PR, Morris JC, Bateman RJ, Dominantly Inherited Alzheimer N (2016) Neurological manifestations of autosomal dominant familial Alzheimer's disease: a comparison of the published literature with the Dominantly Inherited Alzheimer Network observational study (DIAN-OBS). Lancet Neurol 15: 1317–1325.

Terry RD, Masliah E, Salmon DP, Butters N, Deteresa R, Hill R, Hansen LA, Katzman R (2010) Physical basis of cognitive alterations in Alzheimer's disease: synapse loss is the major correlate of cognitive impairment. Annals Neurol 30: 572–580.

The Lancet Neurology (2017) Solanezumab: Too late in mild Alzheimer's disease? Lancet Neurol 16: 97.

Tsushima H, Emanuele M, Polenghi A, Esposito A, Vassalli M, Barberis A, Difato F, Chieregatti E (2015) HDAC6 and RhoA are novel players in Abeta-driven disruption of neuronal polarity. Nat Commun 6: 7781.

Tz-Chong C, Li-Ping C, Chi-Yuan L, Chih-Shung W, Shih-Ping Y (2003) The antiinflammatory and analgesic effects of baicalin in carrageenan-evoked thermal hyperalgesia. Brit J Pharmacol 139: 1146–1152.

Van Dam D, De Deyn PP (2011) Animal models in the drug discovery pipeline for Alzheimer's disease. Br J Pharmacol 164: 1285–1300.

Van Troys M, Huyck L, Leyman SS, Vandekerkhove J, Ampe C (2008) Ins and outs of ADF/cofilin activity and regulation. Eur J Cell Biol 87: 649–667.

Vandenberghe R, Rinne JO, Boada M, Katayama S, Scheltens P, Vellas B, Tuchman M, Gass A, Fiebach JB, Hill D (2016) Bapineuzumab for mild to moderate Alzheimer's disease in two global, randomized, phase 3 trials. Alzheimer's Res Ther 8: 18.

Vepsäläinen S, Koivisto H, Pekkarinen E, Mäkinen P, Dobson G, McDougall GJ, Stewart D, Haapasalo A, Karjalainen RO, Tanila H (2013) Anthocyanin-enriched bilberry and blackcurrant extracts modulate amyloid precursor protein processing and alleviate behavioral abnormalities in the APP/PS1 mouse model of Alzheimer's disease. J Nutr Biochem 24: 360–370.

Villemagne VL, Burnham S, Bourgeat P, Brown B, Ellis KA, Salvado O, Szoeke C, Macaulay SL, Martins R, Maruff P (2013) Amyloid β deposition neurodegeneration and cognitive decline in sporadic Alzheimer's disease: a prospective cohort study. Lancet Neurol 12: 357–367.

Vorhees CV, Williams MT (2006) Morris water maze: procedures for assessing spatial and related forms of learning and memory. Nat Protoc 1: 848–858.

Walsh RN, Cummins RA (1976) The open-field test: a critical review. Psychol Bull 83: 482.

Washington PM, Nicholas M, Maia P, Zapple DN, Burns MP (2014) Experimental traumatic brain injury induces rapid aggregation and oligomerization of amyloid-beta in an Alzheimer's disease mouse model. J Neurotrauma 31: 125.

Wei Y, Liu D, Zheng Y, Li H, Hao C, Ouyang W (2017) Protective effects of kinetin against aluminum chloride and D-galactose induced cognitive impairment and oxidative damage in mouse. Brain Res Bull 134 262–272.

Wioland H, Guichard B, Senju Y, Myram S, Lappalainen P, Jegou A, Romet-Lemonne G (2017) ADF/cofilin accelerates actin dynamics by severing filaments and promoting their depolymerization at both ends. Curr Biol 27: 1956–1967.

World Health Organization (WHO) Dementia. Key facts/14 May 2019 Available at https://www.who.int/news-room/fact-sheets/detail/dementia.

Wu HY, Hudry E, Hashimoto T, Kuchibhotla K, Rozkalne A, Fan Z, Spires-Jones T, Xie H, Arbel-Ornath M, Grosskreutz CL (2010) Amyloid β induces the morphological neurodegenerative triad of spine loss dendritic simplification and neuritic dystrophies through calcineurin activation. J Neurosci 30: 2636–2649.

Wu H, Song A, Hu W, Dai M (2017) The anti-atherosclerotic effect of paeonol against vascular smooth muscle cell proliferation by up-regulation

of autophagy via the AMPK/mTOR signaling pathway. Front Pharmacol 8: 948.

Wyss-Coray T, Rogers J (2012) Inflammation in Alzheimer disease-a brief review of the basic science and clinical literature. CSH Perspect Med 2: a006346.

Xiao Q, Yu W, Tian Q, Fu X, Wang X, Gu M, Lü Y (2017) Chitinase1 contributed to a potential protection via microglia polarization and Aβ oligomer reduction in D-galactose and aluminum-induced rat model with cognitive impairments. Neuroscience 355: 61–70.

Xu F, Xiao H, Liu R, Yang Y, Zhang M, Chen L, Chen Z, Liu P, Huang H (2019) Paeonol ameliorates glucose and lipid metabolism in experimental diabetes by activating akt. Front Pharmacol 10: 261.

Ya-Ping L, Mei Z, Xiang-You H, Hao X, Swaab DF, Rivka R, Jiang-Ning Z (2003) Estrogen receptor alpha-immunoreactive astrocytes are increased in the hippocampus in Alzheimer's disease. Exp Neurol 183: 482–488.

Yamaguchi H, Condeelis J (2007) Regulation of the actin cytoskeleton in cancer cell migration and invasion. Biochim Biophys Acta 1773: 642–652.

Yang J, Ji Y, Mehta P, Bates KA, Sun Y, Wisniewski T (2011) Blocking the apolipoprotein E/amyloid-β interaction reduces fibrillar vascular amyloid deposition and cerebral microhemorrhages in TgSwDI mice. J Alzheimers Dis 24: 269.

Yang N, Higuchi O, Ohashi K, Nagata K, Wada A, Kangawa K, Nishida E, Mizuno K (1998) Cofilin phosphorylation by LIM-kinase 1 and its role in Rac-mediated actin reorganization. Nature 393: 809–812.

Yasunori H, Majewska AK (2005) Dendritic spine geometry: functional implication and regulation. Neuron 46: 529–532.

Yuesong G, Lei C, Viola KL, Lacor PN, Lambert MP, Finch CE, Krafft GA, Klein WL (2003) Alzheimer's disease-affected brain: presence of oligomeric A beta ligands (ADDLs) suggests a molecular basis for reversible memory loss. P Natl Acad Sci USA 100: 10417–10422.

Zhang L, Chen Z, Gong W, Zou Y, Xu F, Chen L, Huang H (2018) Paeonol ameliorates diabetic renal fibrosis through promoting the activation of the Nrf2/ARE pathway via up-regulating Sirt1. Front Pharmacol 9: 512.

Zhang L, Li DC, Liu LF (2019) Paeonol: pharmacological effects and mechanisms of action. Int Immunopharmacol 72: 413–421.

Zhang W, Benson D (2001) Stages of synapse development defined by dependence on F-actin. J Neurosci 21: 5169–5181.

Zhu XL, Chen JJ, Han F, Pan C, Zhuang TT, Cai YF, Lu YP (2018) Novel antidepressant effects of paeonol alleviate neuronal injury with concomitant alterations in BDNF Rac1 and RhoA levels in chronic unpredictable mild stress rats. Psychopharmacology 235: 2177–2191.

SUPPLEMENTAL MATERIAL

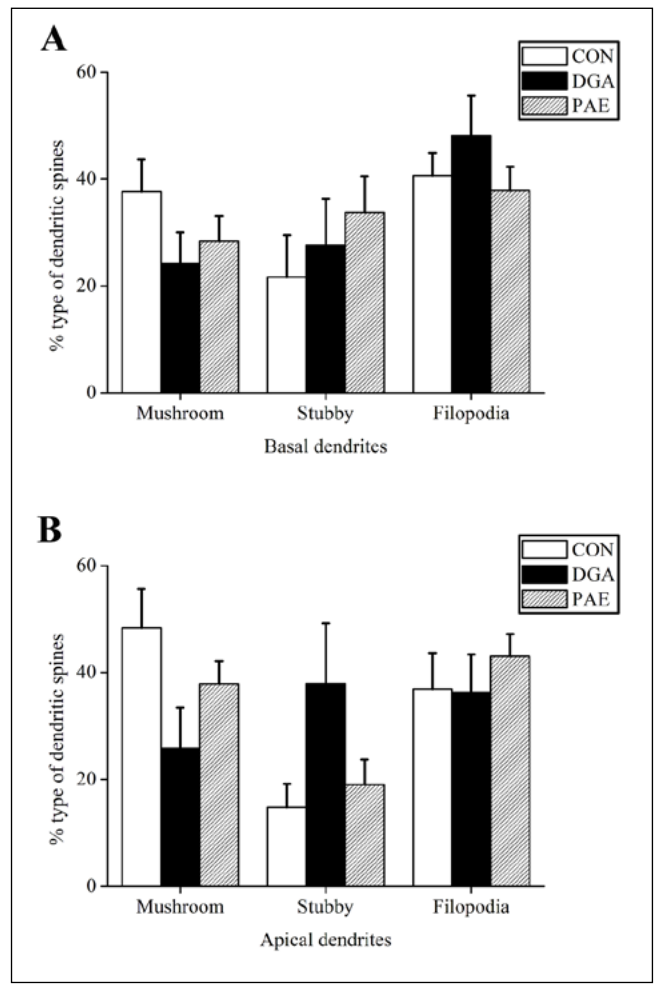

Fig. suppl. Effect of paeonol on percentage type of dendritic spines in frontal cortex. (A) (B) There were no differences in the percentage of any types of dendritic spine found between the groups either in the basal dendrites or in the apical dendrites.